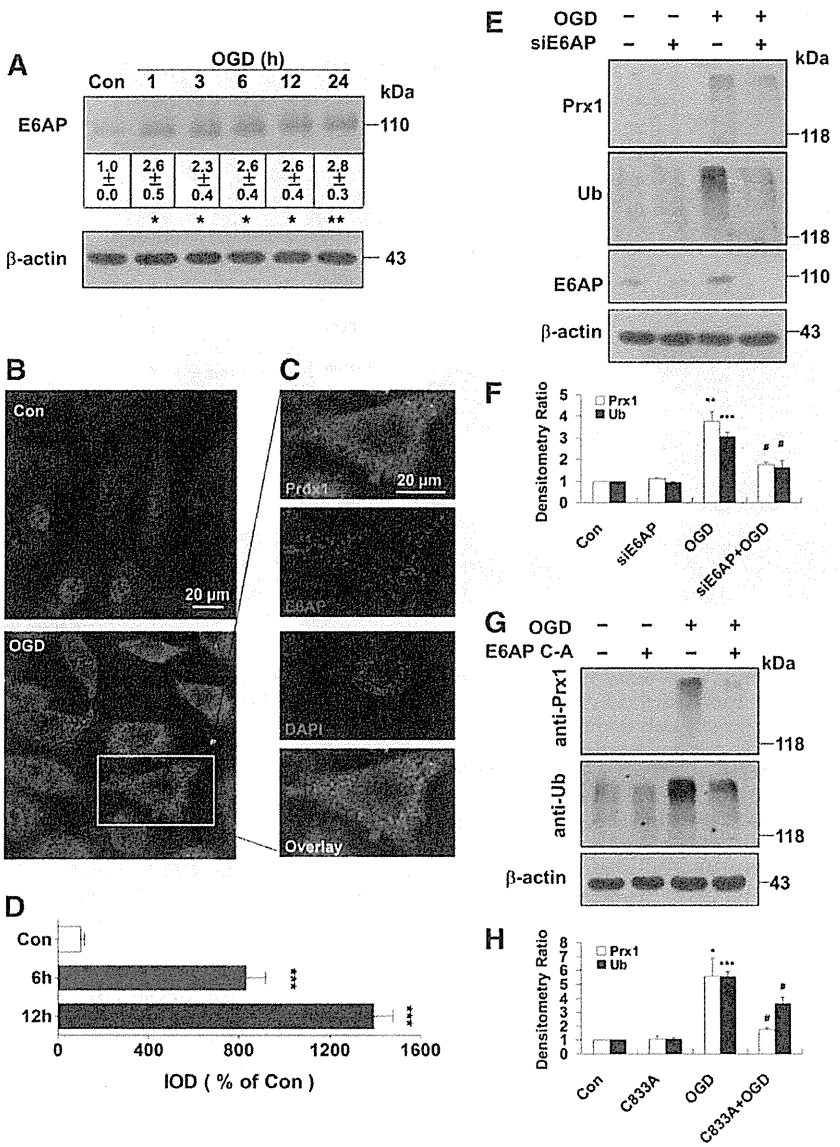

FIG. 5. E6AP activation contributes to the Prx1 stress response after OGD. **(A)** The representative image showing E6AP activation at the indicated time points after OGD treatment. Data are expressed as densitometry ratio of control (mean ± SEM). $*p < 0.05$; $**p < 0.01$ *versus* control. **(B)** Immunocytochemical analysis of E6AP expression after OGD treatment. Laser confocal microscopy demonstrated low to undetectable levels of E6AP in control cells. **(C)** Higher-magnification image of endothelial staining from the *insets* of **(B)**. DAPI counterstaining indicates nuclear localization (blue). Scale bar = 20 μm. **(D)** Quantification of Prx1 immunofluorescence expressed as integrated optical density (IOD). $***p < 0.001$ *versus* control. **(E)** *E6AP* knockdown reduced the OGD-induced formation of multiubiquitinylated proteins. Cells were submitted to *E6AP* knockdown and OGD or the control condition for 6 h. Cell lysates were prepared and resolved by SDS-PAGE. The proteins were immunoblotted with antibodies against Prx1, E6AP, and ubiquitin. **(F)** Quantitative analyses for **(E)** are shown in the bar graph as densitometry ratio of control (mean ± SEM). $**p < 0.01$; $***p < 0.001$ *versus* control; $^{\#}p < 0.05$ *versus* OGD. **(G)** The $E6AP_{C\text{-}A}$ mutant decreased OGD-induced Prx1 ubiquitination in endothelial cells. EA.hy926 cells were cultured and transfected with plasmid DNA encoding the $E6AP_{C\text{-}A}$ mutant or an empty plasmid using Attractene. **(H)** Quantitative analysis of protein levels for **(G)** was performed by densitometry. Data are expressed as densitometry ratio of control (mean ± SEM). $*p < 0.05$; $***p < 0.001$ *versus* control; $^{\#}p < 0.05$ *versus* OGD. Immunodetection of β-actin was used as a loading control. Immunoblots are representative of three independent experiments. E6AP, E6-associated protein. To see this illustration in color, the reader is referred to the web version of this article at www.liebertpub.com/ars

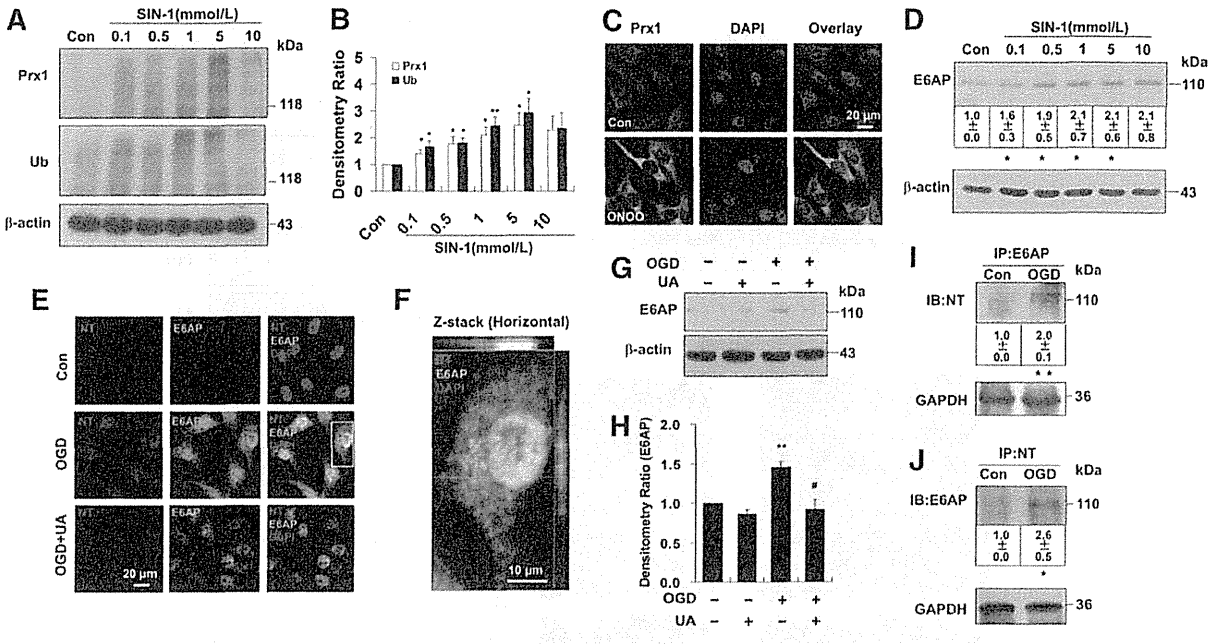

FIG. 6. Nitrosative stress is associated with ubiquitination of Prx1 in endothelial cells. **(A)** The ubiquitination of Prx1 after SIN-1 stimulation in endothelial cells. The blots were labeled with anti-Prx1 or anti-ubiquitin antibody and visualized with the ECL system. Molecular sizes are indicated on the *right*. **(B)** The SIN-1-induced changes in polyubiquitinated Prx1 were quantified and shown in the bar graph as densitometry ratio of control (mean ± SEM). $^{*}p < 0.05$; $^{**}p < 0.01$ *versus* control. **(C)** Immunocytochemical analysis of Prx1 level after $ONOO^-$ treatment by laser confocal microscopy. DAPI counterstaining indicates nuclear localization (blue). **(D)** The effects of SIN-1 treatment on E6AP protein levels were examined in cell lysates of endothelial cells. EA.hy926 endothelial cells were cultured with or without SIN-1 treatment for 6 h at the indicated concentrations. Immunoblots are representative of three independent experiments (mean ± SEM). $^{*}p < 0.05$ *versus* control. **(E)** Fluorescence immunocytochemical staining of E6AP and nitrotyrosine 6 h after OGD in endothelial cells with or without 0.5 m*M* uric acid treatment. DAPI counterstaining indicates nuclear localization (blue). NT, nitrotyrosine; UA, uric acid. **(F)** Higher-magnification image of endothelial staining from the *insets* is shown in **(E)**. **(G)** Effect of uric acid on E6AP expression in endothelial cells following OGD. Immunodetection of β-actin was used as a loading control. **(H)** Quantification of E6AP protein levels was performed using densitometric analysis of the immunoblots in **(G)**. Immunoblots are representative of three independent experiments. Data are expressed as the percentage of values of control (mean ± SEM). $^{**}p < 0.01$ *versus* control; $^{\#}p < 0.05$ *versus* OGD. **(I)** Immunoprecipitation of E6AP from cell lysates of OGD-treated endothelial cells followed by blotting with an anti-nitrotyrosine antibody. $^{**}p < 0.01$ *versus* control. **(J)** The OGD-induced nitration of E6AP was detected by the immunoprecipitation of nitrotyrosine followed by immunoblotting with an anti-E6AP antibody. Immunoblots are representative of three independent experiments (mean ± SEM). $^{*}p < 0.05$ *versus* control. SIN-1, 3-morpholinosydnonimine. To see this illustration in color, the reader is referred to the web version of this article at www.liebertpub.com/ars

striatum (Supplementary Figs. S9 and S10). Staining of brain sections from lentiviral-*GFP*-injected mice with a neuronal nuclear marker (NeuN) (Fig. 8B-d) and an endothelial marker CD31 (Fig. 8B-e, f) indicates that the vector successfully transduced cells in the brain. Although the lentiviral vectors might directly diffused into the brain parenchyma, the present data indicate that lentiviral vectors in cerebral ventricular can diffuse along the neurovascular scaffold. Immunohistochemical analysis of ipsilateral sections revealed stronger GFP fluorescence in tMCAO mice that formed a continuous interendothelial staining pattern that colocalized with CD31 (Fig. 8C, D).

The protective effects of Prx1 against ischemia-induced neurological and functional deficit were evaluated by the rotarod test and neurological score measurements. The neurological scores were decreased significantly, and rotarod time was increased in LV-*Prx1*-treated mice 24 h after tMCAO (Fig. 9A) and the infarct area was reduced accordingly (Fig. 9B). The breakdown products of spectrin and calcineurin were increased after tMCAO (Fig. 9C, D), coincident with BBB leakage (Fig. 9E, F). LV-*Prx1* treatment blocked the degradation of tight junction proteins zonula occludens-1 (ZO-1) and claudin5 (Fig. 9C, D, and G) and significantly reduced BBB leakage (Fig. 9E, F). LV-*Prx1* transduction reduced the $O_2^{\bullet -}$ level assessed from dihydroethidium staining in the penumbra region of mice 24 h after tMCAO (Fig. 9H, I).

Schematic illustration of the mechanisms by which nitrosative stress induces Prx1 ubiquitination during ischemic insult in endothelial cells

We hypothesize that ischemia-induced nitrosative stress causes an early increase in Prx1 production during the adaptive phase, whereas excessive or prolonged ischemia activates E6AP E3 ubiquitin ligase, which targets Prx1 for ubiquitination and degradation during the late phase, thereby degrading the Prx1-related antioxidant defense pathway and

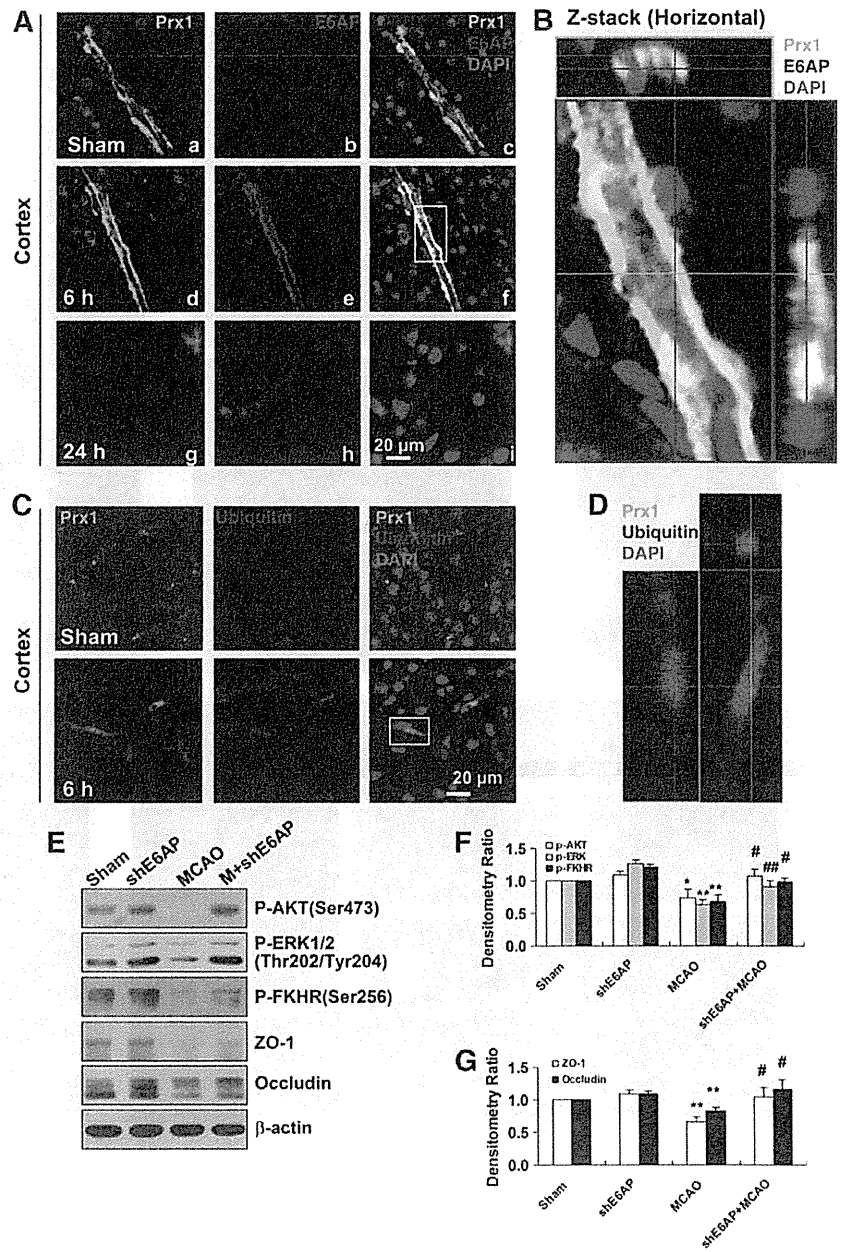

FIG. 7. E6AP activation is associated with Prx1 ubiquitination in brain microvessels of cerebral ischemia mice. (**A**) Double immunohistochemical staining for Prx1 and E6AP in the penumbra after tMCAO. Fluorescence staining for Prx1 (green) and E6AP (red) was performed in ipsilateral brain regions 6 and 24 h after brain ischemic injury in mice. (**B**) The orthogonal projections onto the $x-z$ (*upper*) and $y-z$ (*right*) planes are shown to confirm the colocalization of Prx1 and E6AP throughout the microvessels shown in (**A**). (**C**) Fluorescence immunohistochemical staining of Prx1 and ubiquitin in brain microvessels. Anti-ubiquitin (red) and Prx1 (green) staining was performed 6 h after tMCAO in mice. (**D**) Higher-magnification image of endothelial staining from the *insets* is shown in (**C**). Each image shown is representative of five independent mice. (**E**) The effect of *E6AP* knockdown on neurovascular damage after brain ischemia in mice. The lentivirus *E6AP* shRNA knockdown was used to silence *E6AP* mRNA. The protein extracts from penumbra brain region of mice were processed for western blotting to detect ZO-1, Occludin, and phosphorylated AKT, ERK, FHHR. (**F, G**) Quantitative analysis of protein levels in (**E**) was performed by densitometry. Densitometry values were normalized to the average of all sham values (mean ± SEM, $n=6$). $^{*}p<0.05$; $^{**}p<0.01$ *versus* sham mice; $^{\#}p<0.05$; $^{\#\#}p<0.01$ *versus* vehicle-treated mice. Immunoblotting with an anti-β-actin antibody demonstrated equal protein loading in each lane. tMCAO, transient middle cerebral artery occlusion; ZO-1, zonula occludens-1; shRNA, short hairpin RNA. To see this illustration in color, the reader is referred to the web version of this article at www.liebertpub.com/ars

rendering the endothelial cells in the microvessels susceptible to ischemic damage (Fig. 10).

Discussion

The present study demonstrates that in endothelial cells OGD treatment leads to oxidative and nitrosative stress that engage an early increase in Prx1 production and an antioxidant response. However, more prolonged or severe ischemia-mediated nitrosative stress ubiquitinates Prx1 by the activation of E6AP ligase, thereby degrading this antioxidant defense pathway. The translational studies in mice after MCAO demonstrated that neurovascular protection was coordinated by active Prx1.

Prx1 initiates the antioxidant response by scavenging free radicals formed in response to a diverse array of cellular stresses (40, 44). Upregulation of Prx1 may be secondary to the activation of NF-E2-related factor 2 (Nrf2) (24), as *Prx1* promoter has two antioxidant response elements that are putative binding sites for Nrf2. Indeed, we recently demonstrated that Nrf2 signaling coordinates the defense against ischemia/nitrosative stress in endothelial cells (49).

The ubiquitin–proteasome system is important for protein degradation in eukaryotic cells (19, 42). Unexpectedly, ubiquitin was not highly expressed in control endothelial cells, but high-molecular-weight Prx1-polyubiquitin ladders were observed after OGD or SIN-1 treatment. The aggregation of

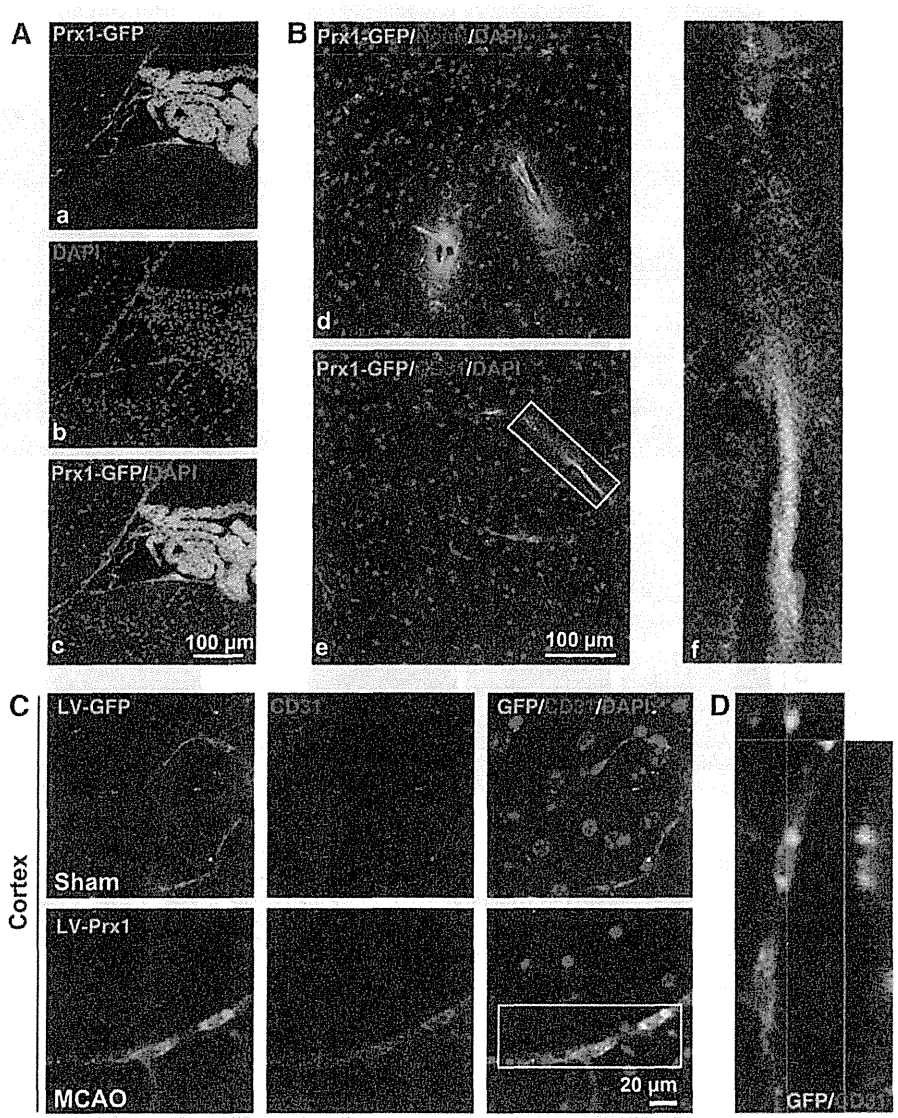

FIG. 8. The brain microvessels are the primary cell type transduced by the LV-*GFP* vector in the ipsilateral side of tMCAO mice. (**A**) The distribution of LV-GFP-Prx1 in the choroid plexus of the mouse brain 2 weeks after intracerebroventricular injection. Images demonstrate successful LV-*GFP-Prx1* transduction in choroid plexus cells. (**B**) The immunohistochemical localization of NeuN-labeled cells (red) in (**d**) and CD31-marked cells (red) in (**e**) were examined in brain cortex of mice. The *inset* (**f**) showing magnified images from (**B-e**) demonstrates the localization of GFP-Prx1 in the microvessels of the brain. (**C**) Representative immunostaining demonstrates that CD31 (red) colocalized with GFP-Prx1 on the ipsilateral side of the brain cortex 24 h after MCAO. (**D**) Representative Z-stack images shown in (**C**). Each image shown is representative of five independently injected mice. NeuN, neuronal nuclear marker. To see this illustration in color, the reader is referred to the web version of this article at www.liebertpub.com/ars

ubiquitinylated Prx1 proteins in endothelial cells after OGD reflects an imbalance between the amount of toxic unfolded proteins and the capacity of the proteasomal system to eliminate them, which may culminate in ER stress. Consistent with our *in vitro* data, there was an increased ubiquitination of Prx1 in brain microvessels of mice following MCAO that was associated with endothelial/microvessel injury. The formation of ubiquitin–protein conjugates (ubi-proteins) may mediate ischemic cell death (19, 51). A time-dependent increase in E6AP after OGD induced Prx1 ubiquitination (33). The upregulation and colocalization of E6AP with Prx1 after OGD was blunted by inhibition of nitrosative stress with uric acid or FeTPPS.

Our results identify E6AP as the E3 ligase that targets Prx1 for degradation in the later phases of OGD. Accordingly, we tested the functional relevance of this pathway in protecting the BBB of mice during tMCAO. Brain ischemia increased E6AP expression in microvessels of the penumbra region. Nitrosative stress from the reaction of NO generated by NO synthases in damaged brain cells and $O_2^{\bullet -}$ generated during ischemia underlays the ischemic cerebral cell death (17, 48). We speculate from our endothelial cell model that ischemic nitrosative stress induced the overproduction of brain microvascular E6AP. Indeed, the computational predictor evaluated 7 potential tyrosine nitration sites of E6AP with high score (Supplementary Fig. S11). Additionally, *S*-nitrosylation has been shown to modify the function of many proteins (1, 32). Therefore, it will also be important to further characterize the protein *S*-nitrosylation of thiol and amine groups during ischemia in the future.

Our finding that inhibition of nitrosative stress and redirection of E6AP restored Prx1 signaling in endothelial cells defines a new vasoprotective mechanism against the damaging consequences of ischemia. This was exemplified by the demonstration that Prx1 overexpression in the intact brain blocked tMCAO-induced neurovascular damage, attenuated

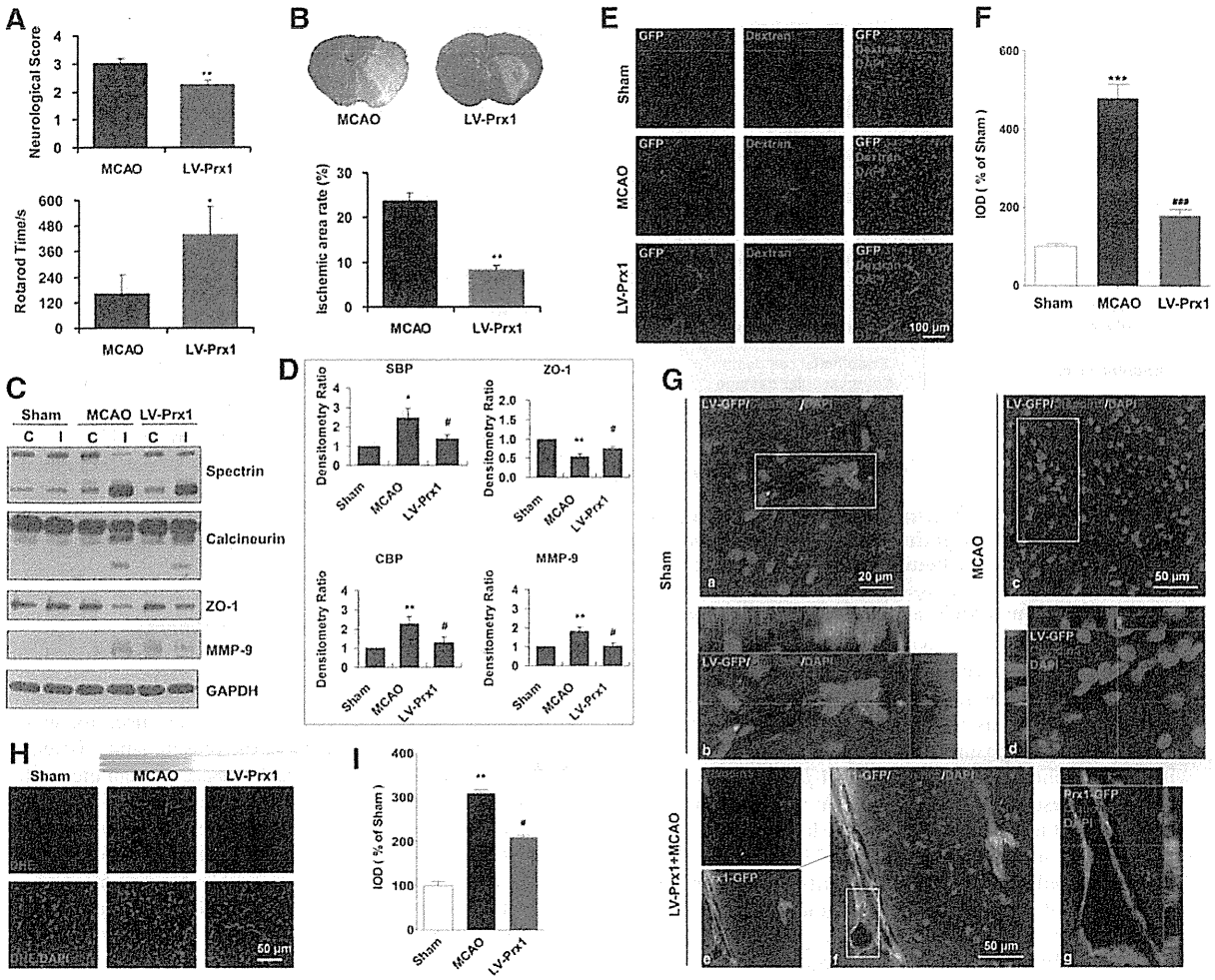

FIG. 9. Lentiviral-mediated delivery of Prx1 protects against neurovascular protection in tMCAO mice. **(A)** Lentiviral-mediated delivery of Prx1 improved neurological functional recovery after focal ischemia. The neurological scores (*upper*) and rotarod test (*lower*) were examined. The data are expressed as the percentage of the values observed in vehicle-treated animals (mean ± SEM, $n = 10$). $^{*}p < 0.05$; $^{**}p < 0.01$ *versus* vehicle-treated mice. **(B)** LV-*Prx1* transduction reduced the infarct area of mice 24 h after tMCAO. The mice were subjected to 45 min of MCAO, and the infarct area was quantified 24 h later in cresyl violet-stained brain sections. The data are expressed as the percentage of the infarct area/total area of each brain section (mean ± SEM, $n = 10$). $^{**}p < 0.01$ *versus* vehicle-treated mice. **(C)** The effect of LV-*Prx1* on neurovascular damage after brain ischemia. The proteins from penumbra brain region of mice were immunoblotted with antibodies against spectrin, calcineurin, ZO-1, and MMP-9, which are indicative antibodies for neurovascular damage. C, contralateral; I, ipsilateral. **(D)** The quantitative analyses are shown in the bar graph as the percentage of values of sham-operated animals (mean ± SEM, $n = 4$). $^{*}p < 0.05$; $^{**}p < 0.01$ *versus* sham mice; $^{\#}p < 0.05$ *versus* vehicle-treated mice. Immunoblotting with an anti-β-actin antibody demonstrated equal protein loading in each lane. SBP, spectrin breakdown products; CBP, calcineurin breakdown products. **(E)** LV-*Prx1* transduction attenuated BBB disruption 24 h after tMCAO. Mice were intravenously injected with Texas red-dextran in saline and perfused 120 min later. *Ex vivo* dextran labeling (red fluorescence) indicated extensive BBB permeability around disrupted brain microvessels in tMCAO mice. **(F)** Quantification of Texas red-dextran immunofluorescence expressed as integrated optical density (IOD). $^{***}p < 0.001$ *versus* sham; $^{\#\#\#}p < 0.001$ *versus* vehicle-treated mice. **(G)** Effect of LV-*Prx1* transduction on the degradation of claudin5. **(a)** Immunostaining with anti-claudin5 (red fluorescence) antibody showed brain ischemia-induced claudin5 degradation **(c, d)** in the microvessels 24 h after tMCAO. LV-*Prx1* transduction reduced the degradation of claudin5 **(e–g)** in the microvessels 24 h after tMCAO. Higher-magnification images of microvessel staining **(b, d, g)** from the *insets* of **(a, c, f)**, respectively. **(H)** The effect of *Prx1* transduction on $O_2^{\bullet -}$ levels, as determined by *in situ* dihydroethidium staining. LV-*Prx1* transduction reduced the $O_2^{\bullet -}$ level in the penumbra region compared to vehicle. Each image shown is representative of five independently injected mice. DHE, dihydroethidium. **(I)** The quantitative analyses of dihydroethidium immunofluorescence are shown in the bar graph. $^{**}p < 0.01$ *versus* sham; $^{\#}p < 0.05$ *versus* vehicle-treated mice. BBB, blood–brain barrier; $O_2^{\bullet -}$, superoxide. To see this illustration in color, the reader is referred to the web version of this article at www.liebertpub.com/ars

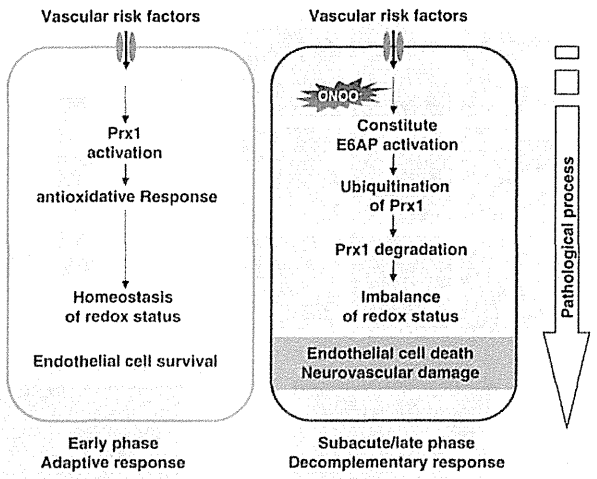

FIG. 10. Schematic illustration of the mechanisms by which nitrosative stress induces Prx1 ubiquitination in endothelial cells during ischemic insult *via* E6AP activation. To see this illustration in color, the reader is referred to the web version of this article at www.liebertpub.com/ars

BBB damage, preserved the ZO-1, and prevented the activation of metalloproteinases (MMPs). This is similar to the reports that Prx1 was required also for neurovascular cell survival during exposure to pathogenic proteins associated with brain ischemia or with amyloid-β expression in neurons (30). These results are consistent with the finding that *Prx1*-deficient mice suffer embryonic lethality because they lack essential antioxidant function (25, 34, 39). Although the neurovascular cells might be a critical issue during the earlier phase of brain ischemia, the functional coupling and collaborations among the capillaries, glia, and neurons of the brain should be taken into consideration (9, 37). For instance, recent studies highlight that pericyte loss causes BBB breakdown and neurodegeneration (2, 36). Therefore, how Prx1-mediated vascular protection contributed to the neuronal survival in the present study, however, is a topic for further investigation. Prx1 protein levels can prevent excessive ROS accumulation by interaction with thioredoxin to detoxify hydrogen peroxide (H_2O_2), $ONOO^-$, and a range of organic hydroperoxides (34). We found further that LV transduction reduced $O_2^{\bullet -}$ formation in the ipsilateral region of the ischemia brain, which might be a consequence of ERK and FKHR activation by Prx1. Indeed, Prxs participate in a very wide range of reactions, including neuronal differentiation, cell signaling, molecular chaperoning, and mitochondrial function, in both catalytic-dependent and catalytic-independent manners and can interact with JNK, c-Abl, and apoptosis signal-regulating kinase 1 (ASK1) in a redox-regulated manner (11, 14, 21, 23). Here, ipsilateral sections showed stronger GFP fluorescence in cerebral vessels of tMCAO mice, it might due to the changes of structural integrity in ischemic region, where dividing cell also largely accumulated (12, 20).

In summary, our studies identify an intracellular link between nitrosative stress and Prx1 signaling in endothelial cells following ischemia-like injury. Our description of an early ischemia-induced activation of beneficial Prx1 generation followed by subsequent inactivation represents a previously undescribed, nitrosative stress-dependent process mediated by E6AP-dependent Prx1 ubiquitination and subsequent endothelial barrier damage. Since Prx1 protected against oxidative stress in endothelial cells to reduce injury after ischemia, both *in vitro*- and *in vivo*-specific inducers of the Prx1 pathway, or mechanisms to prevent its degradation, may be targeted for therapeutic benefit in neurovascular disorders.

Materials and Methods

Reagents

Dulbecco's modified Eagle's medium (DMEM) and fetal bovine serum were purchased from Gibco. Alexa Fluor 488-conjugated anti-rabbit IgG and Alexa Fluor 594-conjugated anti-mouse IgG were obtained from Invitrogen. Uric acid was obtained from Wako. 5,10,15,20-Tetrakis-[4-sulfonatophenyl]-porphyrinato-iron[III] (FeTPPS; Calbiochem) was used as a specific $ONOO^-$ decomposition catalyst. Unless otherwise stated, all reagents and chemicals were obtained from Sigma-Aldrich.

OGD exposure and experimental treatments of cell cultures

EA.hy926 cells (16, 43), HBMECs, and mouse brain microvascular endothelial cells (bEnd.3) were used for western blot or immunocytochemistry in the present study. Briefly, in the oxygen and glucose deprivation phase, the culture medium was replaced and washed with glucose-free Hank's balanced salt solution, after which the cultures were placed in an airtight experimental hypoxia chamber (Billups-Rothenberg) containing a gas mixture comprising 95% N_2 and 5% CO_2. To mimic an ischemia-like condition *in vitro*, cell cultures were exposed to OGD for 1, 3, 6, 12, and 24 h. Cells without OGD served as controls.

Two-dimensional gel electrophoresis

Approximately 450 μg of protein was resuspended in a rehydration solution [8 *M* Urea, 2% CHAPS, 20 m*M* DTT, 0.2% Biolyte (pH range 3–10), and 0.2% Bromphenol blue] and applied to 17-cm pH 3–10 nonlinear gradient immobiline strips for isoelectric focusing. Isoelectric focusing was performed using Protean IEF Cell (Bio-Rad), and the proteins in the IPG strips were subsequently placed on a 12% uniform sodium dodecyl sulfate (SDS)–polyacrylamide gel. The gels were silver stained and scanned with an Image Scanner in transmission mode, after which image analysis was conducted with two-dimensional PDquest (Bio-Rad). The two-dimensional gel electrophoresis was repeated three times using independently grown cultures.

In-gel digestion and mass spectrometry analysis

The in-gel digestion of proteins for mass spectrometric characterization was performed as published previously (47). After the tryptic peptide mixture was dissolved with 0.5% trifluoroacetic acid, peptide mass analysis was performed using an AB4800 MALDI-TOF/TOF mass spectrometer (Applied Biosystems). The mass spectra were externally calibrated with a peptide standard from Applied Biosystems. Based on the National Center for Biotechnology Information

(NCBI) human databases, the mass spectra were analyzed with a 50 ppm mass tolerance by GPS Explorer version 2.0.1 and Mascot version 1.9.

Plasmid constructs and transfections

The EA.hy926 or HBMEC endothelial cells were cultured in six-well plates in the growth medium and transfected with plasmid DNA encoding *Prx1*, *siPrx1*, *siE6AP*, *pRK5-HA-Ubiquitin-K48R* (17604; Addgene), or an empty plasmid control using Attractene (Qiagen). After transfection for 2 days, the cells were collected for related experiments. To express the active-site cysteine-to-alanine mutant of E6AP in endothelial cells, *p3869HA-E6AP C833A* cells (8649; Addgene) were used. The C-A mutation was introduced at the site of E6AP C833 (22, 27). The *K48R mutant ubiquitin* was obtained from Dr. Guanghui Wang (Soochow University) (27). All the constructs were confirmed by sequencing.

Lentiviral vectors preparation for brain delivery

To construct a lentiviral vector expressing Prx1, two complementary *Prx1* DNA oligonucleotides were synthesized and inserted into the *Eco*RI-*Bam*HI site of transfer vector *pCDH-CMV-MCS-EF1-copGFP* under the control of promoter *CMV*. The constructed vector was transformed into DH5a *Escherichia coli* and isolated with minipreps plasmid purification system (Promega). A large production of LV-*Prx1* was prepared by transfection of human kidney 293T cells. In brief, 293T cells were cotransfected with a mixture containing packaging plasmid (*pCD/NL-BH*DDD*), envelope plasmid (*pLTR-G*), and transfer vector and Trans-EZ. For high-titer virus stocks, the supernatant of cells was collected at 72 h after transfection, low-speed centrifuged, filtered, and ultracentrifuged. The titer of LV-*Prx1* stock was determined by transduction of HOS cells with serial dilutions of concentrated lentivirus and analyzing integrated viral DNA copies per cell by quantitative polymerase chain reaction. The lentiviral vectors coding for *GFP* without *Prx1* were prepared in a similar manner, as described above, and used as a control (LV-*GFP*). In addition, we used a lentivirus-mediated RNA interference approach to achieve the inhibition of E6AP levels in the brain. The short hairpin RNA (shRNA)-mediated *Ube3a* knockdown vectors were constructed by subcloning the U6 promoter-sh-*Ube3a* cassette into the *Age*I-*Eco*RI sites of the *pLenti-CMV* vector.

The lentiviral vector encoding mouse *Prx1* (LV-*GFP-Prx1*), LV-*GFP*, or sh-*E6AP* was injected into the right lateral ventricle over a 10-min duration using a Hamilton microsyringe with the coordinates of 0.5 mm caudal to the bregma, 1 mm lateral to the midline, and 3 mm depth from the skull surface under the guidance of a stereotaxic instrument. Two weeks after the introduction of the viral vectors, the MCAO mice model was prepared as previously reported (51). All lentivirus batches used for experiments had comparable titers ranging from 1×10^8 to 1×10^9 integration units/ml. Virus suspensions were stored at −80°C until use and were briefly centrifuged and kept on ice immediately before injection.

RNA interference

Prx1 siRNAs or *E6AP* siRNAs was introduced into EA.hy926 cells with the transfection medium according to the manufacturer's instructions. The control set of EA.hy926 cells was transfected with nontargeted siRNAs. The cells were collected for experiments 72 h after transfection. Knockdown was confirmed with western blotting using whole cell lysates. si*Prx1* (sc-36177) and scramble negative control (sc-37007) were obtained from Santa Cruz Biotechnology: si*E6AP* (sense), 5′-GCCCAGACACAGAA AGGUUTT-3′; scramble negative control (siCont-1, sense), 5′-UUGCGGGUCUAAUCACCGATT-3′.

Annexin V/PI flow cytometry analysis

Flow cytometric assays to evaluate apoptosis by Annexin V/PI (BioVision) staining were performed essentially as previously described, following the manufacturer's instruction. Briefly, endothelial cells were transfected with *Prx1* siRNAs for 48 h before exposure to 6 h OGD. Annexin V-FITC and PI were added to the cell suspension and incubated at room temperature for 10 min in the dark. For each sample, at least 1×10^4 cells were analyzed using a FACS-Calibur flow cytometer (BD Biosciences).

TUNEL assay

In situ DNA fragmentation was assessed using a TUNEL staining combined with 4′,6-diamidino-2-phenylindole (DAPI) counterstain. Images were recorded after counterstaining with DAPI (nuclei marker), and endothelial cells were identified by phase image. Endothelial cells were imaged using 20× objectives. The apoptotic response was expressed as the percentage of TUNEL-positive endothelial cells/the total number of nuclei counted after DAPI staining. The results represented the average of a minimum of three experiments, and a minimum of 600 cells were counted per experiment.

Cell fractionation, immunoprecipitation, and immunoblotting analysis

Immunoblotting was carried out in endothelial cell lysates after determination of protein concentrations using the Bradford's solution. The cell lysates containing equivalent amounts of protein were applied to 10%–13.5% acrylamide denaturing gels (SDS-polyacrylamide gel electrophoresis [PAGE]) (15). Proteins were then transferred to an immobilon polyvinylidene difluoride membrane for 1 h at 50 V. Membranes were blocked in 20 m*M* Tris-HCl (PH 7.4), 150 m*M* NaCl, and 0.1% Tween 20 (TBS-T) containing 5% fat-free milk powder for 1 h and immunodetected with antibodies to HSP27 monoclonal antibody (1:1000), Prx1 polyclonal antibody (1:5000), (Abcam); HO-1 (1:1000), Phospho-AKT (1:1000), Phospho-ERK (1:3000), Phospho-JNK (1:1000), Phospho-P38 (1:1000), Phospho-FKHR (1:3000), and cleaved Caspase-3 (1:1000, polyclonal antibody; Cell Signaling Technology); procaspase-3 (1:2000), PARP-1 (1:2000), and ubiquitin (1:1000, polyclonal antibody; Santa Cruz Biotechnology); ZO-1 and Occludin (1:1000; Invitrogen); E6AP (1:3000) and β-actin (1:5000, monoclonal antibody; Sigma-Aldrich). After incubation for 12 h, membranes were incubated with the appropriate horseradish peroxidase-conjugated secondary antibody. Immunoreactivity was visualized by enhanced chemiluminescence (Amersham Life Science). The Prx1 ubiquitylation assays were performed essentially as described previously (46). Briefly, cells were treated with 5 μ*M* MG132 (Calbiochem)

or with dimethyl sulfoxide (DMSO; control) for 30 min before OGD. Immunoprecipitates were analyzed by immunoblotting, using either anti-ubiquitin or anti-Prx1 antibody to detect ubiquitylated Prx1. In addition, E6AP immunoprecipitates from the lysates were probed with anti-nitrotyrosine antibody.

Experimental animals

Male C57 mice, weighing 20–23 g, were obtained from the Zhejiang Medical Animal Centre (Hangzhou, China). Mice were housed under climate-controlled conditions with a 12-h light/dark cycle and provided with standard food and water. Animals were acclimated to their environment for at least 1 week before initiating the experimental protocols. All experimental protocols and animal handling procedures were performed in accordance with the National Institutes of Health (NIH) guidelines for the care and use of laboratory animals and were approved by the Committee for Animal Experiments at the Zhejiang University in China.

tMCAO model

The transient/reperfusion MCAO model was used to resemble stroke in humans (3, 5), and the surgery was carried out as previously described (18). Animal procedures were approved by the Committee on Animal Experiments at the Zhejiang University. The rectal temperature was monitored throughout the surgery, and the body temperature was maintained at 37°C ± 0.5°C with a heating pad. Neurological deficit tests were carried out at 24 h after tMCAO, including neurological scores and rotarod test. Neurological scores were determined 24 h after tMCAO using a previously described scoring system (45). Rotarod test, which started 3 days before the surgery to train five times every day, was performed to examine the motor coordination. The rotarod time (s) that mice persisted on the rotarod after ischemia was recorded; the data were expressed as the mean duration of five trials at 24 h after tMCAO. The brain infarct area of mice 24 h after ischemia was evaluated from scanned digital images of Nissl-stained brain sections using Image J software (NIH).

Evaluation of BBB damage

The loss of BBB integrity was also verified by the leakage of Texas red-conjugated dextran from microvessels after intravenous injection. Texas red-dextran (70 kDa) solution (0.1% in phosphate-buffered saline [PBS], 5 ml/kg) was intravenously administered *via* the tail vein at 22 h after the onset of MCAO. The mice were perfused transcardially with saline as above. After decapitation, brains were prepared according to the immunohistochemical methods, and Texas red-dextran leakage was determined by immunofluorescence staining (red fluorescence).

Confocal immunofluorescence staining and analysis

For immunofluorescence analysis in cultured endothelial cells, cells were fixed in 4% formaldehyde/PBS as previously reported (16). Cells were labeled with Prx1 (1:300, polyclonal antibody; Abcam), Nitrotyrosine (1:200, monoclonal antibody; Millipore), E6AP (1:300, polyclonal antibody; Invitrogen), and ubiquitin (1:200, monoclonal antibody; Cell Signaling Technology), followed by immunofluorescence using a standard protocol from PerkinElmer Life Sciences, Inc. Nuclei were stained with DAPI dihydrochloride bisbenzimide (5 μM). Immunolocalization and changes in Prx1, E6AP, and nitrotyrosine in cultured endothelial cells were visualized by confocal microscopy (Zeiss LSM 510).

For immunohistochemistry, mice were anesthetized at the time of sacrifice and transcardially perfused with 4% paraformaldehyde in PBS as previously described (16). The whole brains were immediately removed and post-fixed overnight at 4°C. Then, brains were cut into 35-μm-thick serial sections using a vibratome. Sections were incubated at room temperature in PBS with 0.01% Triton-X100 for 30 min and for 1 h in 3% bovine serum albumin (BSA) in PBS. For immunolabeling, the brain slices were incubated with antibodies targeting Prx1 (1:300; Abcam), CD31 (1:200; Santa Cruz Biotechnology), Claudin5 (1:200; Invitrogen), E6AP (1:300; Sigma-Aldrich), NeuN (1:300), and Nitrotyrosine (1:200) (Millipore) overnight at 4°C. After washing, the sections were incubated with Alexa fluor 488-conjugated anti-rabbit IgG (1:400) and Alexa fluor 594-conjugated anti-mouse IgG (1:400) (Invitrogen) in (Tris-NaCl-blocking) TNB buffer (1:400). In addition, the oxidative fluorescent indicator dihydroethidium was used to evaluate *in situ* $O_2^{\bullet -}$ generation as previously reported (45). Immunofluorescence was visualized by using a Zeiss LSM 510 confocal microscope.

Statistical analysis

The data were analyzed with *t*-tests when means between two groups were compared. For multigroup comparisons, statistical significance was determined using one-way ANOVA followed by a *post hoc* Tukey's test or Dunnett's comparison to control. All data are expressed as the mean ± SEM. A value of $p < 0.05$ was considered to be significant.

Acknowledgments

This work was supported in part by the National Natural Science Foundation of China (81120108023, 91232705, 81202533); the Zhejiang Provincial Qianjiang Talent Plan (2012R10036); the Zhejiang Provincial Natural Science Foundation of China (R2100281); NIH grants (NHLBI HL-68686, NIDDK DK-49870, and DK-36079).

Author Disclosure Statement

No competing financial interests exist.

References

1. Aracena P, Tang W, Hamilton SL, and Hidalgo C. Effects of S-glutathionylation and S-nitrosylation on calmodulin binding to triads and FKBP12 binding to type 1 calcium release channels. *Antioxid Redox Signal* 7: 870–881, 2005.
2. Armulik A, Genové G, Mäe M, Nisancioglu MH, Wallgard E, Niaudet C, He L, Norlin J, Lindblom P, Strittmatter K, Johansson BR, and Betsholtz C. Pericytes regulate the blood-brain barrier. *Nature* 468: 557–561, 2010.
3. Braeuninger S and Kleinschnitz C. Rodent models of focal cerebral ischemia: procedural pitfalls and translational problems. *Exp Transl Stroke Med* 1: 8, 2009.
4. Brunet Simioni M, De Thonel A, Hammann A, Joly AL, Bossis G, Fourmaux E, Bouchot A, Landry J, Piechaczyk M, and Garrido C. Heat shock protein 27 is involved in SUMO-2/3 modification of heat shock factor 1 and thereby

modulates the transcription factor activity. *Oncogene* 28: 3332–3344, 2009.
5. Carmichael ST. Rodent models of focal stroke: size, mechanism, and purpose. *NeuroRx* 2: 396–409, 2005.
6. Chae HZ, Kang SW, and Rhee SG. Isoforms of mammalian peroxiredoxin that reduce peroxides in presence of thioredoxin. *Methods Enzymol* 300: 219–226, 1999.
7. Chae HZ, Oubrahim H, Park JW, Rhee SG, and Chock PB. Protein glutathionylation in the regulation of peroxiredoxins: a family of thiol-specific peroxidases that function as antioxidants, molecular chaperones, and signal modulators. *Antioxid Redox Signal* 16: 506–523, 2012.
8. Coe H, Bedard K, Groenendyk J, Jung J, and Michalak M. Endoplasmic reticulum stress in the absence of calnexin. *Cell Stress Chaperones* 13: 497–507, 2008.
9. del Zoppo GJ. . The neurovascular unit, matrix proteases, and innate inflammation. *Ann N Y Acad Sci* 1207: 46–49, 2010.
10. Fisher AB. Peroxiredoxin 6: a bifunctional enzyme with glutathione peroxidase and phospholipase A_2 activities. *Antioxid Redox Signal* 15: 831–844, 2011.
11. Gan Y, Ji X, Hu X, Luo Y, Zhang L, Li P, Liu X, Yan F, Vosler P, Gao Y, Stetler RA, and Chen J. Transgenic overexpression of peroxiredoxin-2 attenuates ischemic neuronal injury *via* suppression of a redox-sensitive pro-death signaling pathway. *Antioxid Redox Signal* 17: 719–732, 2012.
12. Geraerts M, Eggermont K, Hernandez-Acosta P, Garcia-Verdugo JM, Baekelandt V, and Debyser Z. Lentiviral vectors mediate efficient and stable gene transfer in adult neural stem cells *in vivo*. *Hum Gene Ther* 17: 635–650, 2006.
13. Girouard H, Park L, Anrather J, Zhou P, and Iadecola C. Cerebrovascular nitrosative stress mediates neurovascular and endothelial dysfunction induced by angiotensin II. *Arterioscler Thromb Vasc Biol* 27: 303–309, 2007.
14. Guo X, Yamada S, Tanimoto A, Ding Y, Wang KY, Shimajiri S, Murata Y, Kimura S, Tasaki T, Nabeshima A, Watanabe T, Kohno K, and Sasaguri Y. Overexpression of peroxiredoxin 4 attenuates atherosclerosis in apolipoprotein E knockout mice. *Antioxid Redox Signal* 17: 1362–1375, 2012.
15. Han F, Ali Raie A, Shioda N, Qin ZH, and Fukunaga K. Accumulation of beta-amyloid in the brain microvessels accompanies increased hyperphosphorylated tau proteins following microsphere embolism in aged rats. *Neuroscience* 153: 414–427, 2008.
16. Han F, Chen YX, Lu YM, Huang JY, Zhang GS, Tao RR, Ji YL, Liao MH, Fukunaga K, and Qin ZH. Regulation of the ischemia-induced autophagy-lysosome processes by nitrosative stress in endothelial cells. *J Pineal Res* 51: 124–135, 2011.
17. Han F, Shirasaki Y, and Fukunaga K. Microsphere embolism-induced endothelial nitric oxide synthase expression mediates disruption of the blood-brain barrier in rat brain. *J Neurochem* 99: 97–106, 2006.
18. Han F, Tao RR, Zhang GS, Lu YM, Liu LL, Chen YX, Lou YJ, Fukunaga K, and Hong ZH. Melatonin ameliorates ischemic-like injury-evoked nitrosative stress: Involvement of HtrA2/PED pathways in endothelial cells. *J Pineal Res* 50: 281–291, 2011.
19. Hu BR, Martone ME, Jones YZ, and Liu CL. Protein aggregation following transient cerebral ischemia. *J Neurosci* 20: 3191–3199, 2000.
20. Jakobsson J and Lundberg C. Lentiviral vectors for use in the central nervous system. *Mol Ther* 13: 484–493, 2006.
21. Kakihana T, Nagata K, and Sitia R. Peroxides and peroxidases in the endoplasmic reticulum: integrating redox homeostasis and oxidative folding. *Antioxid Redox Signal* 16: 763–771, 2012.
22. Kao WH, Beaudenon SL, Talis AL, Huibregtse JM, and Howley PM. Human papillomavirus type 16 E6 induces self-ubiquitination of the E6AP ubiquitin-protein ligase. *J Virol* 74: 6408–6417, 2000.
23. Kim SY, Kim TJ, and Lee KY. A novel function of peroxiredoxin 1 (Prx-1) in apoptosis signal-regulating kinase 1 (ASK1)-mediated signaling pathway. *FEBS Lett* 582: 1913–1918, 2008.
24. Kim YJ, Ahn JY, Liang P, Ip C, Zhang Y, and Park YM. Human prx1 gene is a target of Nrf2 and is upregulated by hypoxia/reoxygenation: implication to tumor biology. *Cancer Res* 67: 546–554, 2007.
25. Kisucka J, Chauhan AK, Patten IS, Yesilaltay A, Neumann C, Van Etten RA, Krieger M, and Wagner DD. Peroxiredoxin1 prevents excessive endothelial activation and early atherosclerosis. *Circ Res* 103: 598–605, 2008.
26. Leblanc GG, Golanov E, Awad IA, and Young WL. Biology of Vascular Malformations of the Brain NINDS Workshop Collaborators. Biology of vascular malformations of the brain. *Stroke* 40: e694–e702, 2009.
27. Liu C, Fei E, Wang H, Tao R, Iwata A, Nukina N, Zhou J, and Wang G. Assembly of lysine 63-linked ubiquitin conjugates by phosphorylated-synuclein implies lewy body biogenesis. *J Biol Chem* 282: 14558–14566, 2007.
28. Liu G, Feinstein SI, Wang Y, Dodia C, Fisher D, Yu K, Ho YS, and Fisher AB. Comparison of glutathione peroxidase 1 and peroxiredoxin 6 in protection against oxidative stress in the mouse lung. *Free Radic Biol Med* 49: 1172–1181, 2010.
29. Liu QB, Liu LL, Lu YM, Tao RR, Huang JY, Han F, and Lou YJ. The induction of reactive oxygen species and loss of mitochondrial Omi/HtrA2 is associated with S-nitrosoglutathione-induced apoptosis in human endothelial cells. *Toxicol Appl Pharmacol* 244: 374–384, 2010.
30. Manczak M, Mao P, Calkins MJ, Cornea A, Reddy AP, Murphy MP, Szeto HH, Park B, and Reddy PH. Mitochondria-targeted antioxidants protect against amyloid-beta toxicity in Alzheimer's disease neurons. *J Alzheimers Dis* 20: S609–S631, 2010.
31. Mowbray AL, Kang DH, Rhee SG, Kang SW, and Jo H. Laminar shear stress up-regulates peroxiredoxins (PRX) in endothelial cells: PRX 1 as a mechanosensitive antioxidant. *J Biol Chem* 283: 1622–1627, 2008.
32. Nakamura T and Lipton SA. S-nitrosylation of critical protein thiols mediates protein misfolding and mitochondrial dysfunction in neurodegenerative diseases. *Antioxid Redox Signal* 14: 1479–1492, 2011.
33. Nasu J, Murakami K, Miyagawa S, Yamashita R, Ichimura T, Wakita T, Hotta H, Miyamura T, Suzuki T, Satoh T, and Shoji I. E6AP ubiquitin ligase mediates ubiquitin-dependent degradation of peroxiredoxin 1. *J Cell Biochem* 111: 676–685, 2010.
34. Neumann CA, Krause DS, Carman CV, Das S, Dubey DP, Abraham JL, Bronson RT, Fujiwara Y, Orkin SH, and Van Etten RA. Essential role for the peroxiredoxin Prdx1 in erythrocyte antioxidant defence and tumour suppression. *Nature* 424: 561–565, 2003.
35. Pitts A, Dailey K, Newington JT, Chien A, Arseneault R, Cann T, Thompson LM, and Cumming RC. Dithiol based compounds maintain expression of antioxidant protein

peroxiredoxin 1 that counteracts toxicity of mutant hungtington. *J Biol Chem* 287: 22717–22729, 2012.
36. Quaegebeur A, Segura I, and Carmeliet P. Pericytes: blood-brain barrier safeguards against neurodegeneration? *Neuron* 68: 321–323, 2010.
37. Quaegebeur A, Lange C, and Carmeliet P. The neurovascular link in health and disease: molecular mechanisms and therapeutic implications. *Neuron* 71: 406–424, 2011.
38. Rabilloud T, Heller M, Gasnier F, Luche S, Rey C, Aebersold R, Benahmed M, Louisot P, and Lunardi J. Proteomics analysis of cellular response to oxidative stress. Evidence for *in vivo* overoxidation of peroxiredoxins at their active site. *J Biol Chem* 277: 19396–19401, 2002.
39. Rani V, Neumann CA, Shao C, and Tischfield JA. Prdx1 deficiency in mice promotes tissue specific loss of heterozygosity mediated by deficiency in DNA repair and increased oxidative stress. *Mutat Res* 735: 39–45, 2012.
40. Riddell JR, Maier P, Sass SN, Moser MT, Foster BA, and Gollnick SO. Peroxiredoxin 1 stimulates endothelial cell expression of VEGF *via* TLR4 dependent activation of HIF-1α. *PLoS One* 7: e50394, 2012.
41. Rizzo MT and Leaver HA. Brain endothelial cell death: modes, signaling pathways, and relevance to neural development, homeostasis, and disease. *Mol Neurobiol* 42: 52–63, 2010.
42. Rott R, Szargel R, Haskin J, Bandopadhyay R, Lees AJ, Shani V, and Engelender S. α-Synuclein fate is determined by USP9X-regulated monoubiquitination. *Proc Natl Acad Sci U S A* 108: 18666–186671, 2011.
43. Satoh M, Fujimoto S, Haruna Y, Arakawa S, Horike H, Komai N, Sasaki T, Tsujioka K, Makino H, and Kashihara N. NAD (P) h oxidase and uncoupled nitric oxide syntase are major sources of glomerular superoxide in rats with experimental diabetic nephropathy. *Am J Physiol Renal Physiol* 288: F1144–F1152, 2005.
44. Schreibelt G, van Horssen J, Haseloff RF, Reijerkerk A, van der Pol SM, Nieuwenhuizen O, Krause E, Blasig IE, Dijkstra CD, Ronken E, and de Vries HE. Protective effects of peroxiredoxin-1 at the injured blood-brain barrier. *Free Radic Biol Med* 45: 256–264, 2008.
45. Shioda N, Han F, Moriguchi S, and Fukunaga K. Constitutively active calcineurin mediates delayed neuronal death through Fas-ligand expression *via* activation of NFAT and FKHR transcriptional activities in mouse brain ischemia. *J Neurochem* 102: 1506–1517, 2007.
46. Shirakura M, Murakami K, Ichimura T, Suzuki R, Shimoji T, Fukuda K, Abe K, Sato S, Fukasawa M, Yamakawa Y, Nishijima M, Moriishi K, Matsuura Y, Wakita T, Suzuki T, Howley PM, Miyamura T, and Shoji I. E6AP ubiquitin ligase mediates ubiquitylation and degradation of hepatitis C virus core protein. *J Virol* 81: 1174–1185, 2007.
47. Sultana R, Perluigi M, Newman SF, Pierce WM, Cini C, Coccia R, and Butterfield DA. Redox proteomic analysis of carbonylated brain proteins in mild cognitive impairment and early Alzheimer's disease. *Antioxid Redox Signal* 12: 327–336, 2010.
48. Tan KH, Harrington S, Purcell WM, and Hurst RD. Peroxinitrite mediates nitric oxide-induced blood-brain barrier damage. *Neurochem Res* 29: 579–587, 2004.
49. Tao RR, Ji YL, Lu YM, Fukunaga K, and Han F. Targeting nitrosative stress for neurovascular protection: new implications in brain diseases. *Curr Drug Targets* 13: 272–284, 2012.
50. Wilcox CS and Pearlman A. Chemistry and antihypertensive effects of tempol and other nitroxides. *Pharmacol Rev* 60: 418–469, 2008.
51. Zhang GS, Tian Y, Huang JY, Tao RR, Liao MH, Lu YM, Ye WF, Wang R, Fukunaga K, Lou YJ, and Han F. The γ-Secretase blocker DAPT reduces the permeability of the blood-brain barrier by decreasing the ubiquitination and degradation of occludin during permanent brain ischemia. *CNS Neurosci Ther* 19: 53–60, 2012.

Address correspondence to:
Dr. Feng Han
Institute of Pharmacology, Toxicology and Biochemical Pharmaceutics
Zhejiang University
Hangzhou 310058
China

E-mail: changhuahan@zju.edu.cn

Date of first submission to ARS Central, April 18, 2013; date of final revised submission, November 12, 2013; date of acceptance, December 2, 2013.

Abbreviations Used

ASK1 = apoptosis signal-regulating kinase 1
BBB = blood–brain barrier
DAPI = 4′,6-diamidino-2-phenylindole
DMEM = Dulbecco's modified Eagle's medium
E6AP = E6-associated protein
ER = endoplasmic reticulum
FKHR = forkhead transcription factor Foxo1
H_2O_2 = hydrogen peroxide
HBMEC = human brain microvascular endothelial cell
HO-1 = heme oxygenase-1
HSP27 = heat shock protein 27
JNK = c-Jun N-terminal kinase
MALDI-TOF = matrix-assisted laser desorption/ionization-time-of-flight
mHtt = mutant Hungtington
MMPs = metalloproteinases
NeuN = neuronal nuclear marker
NO = nitric oxide
Nrf2 = NF-E2-related factor 2
$O_2^{\bullet-}$ = superoxide
OGD = oxygen–glucose deprivation
$ONOO^-$ = peroxynitrite
PAGE = polyacrylamide gel electrophoresis
PARP = poly ADP-ribose polymerase
PBS = phosphate-buffered saline
PI = propidium iodide
Prx = peroxiredoxin
ROS = reactive oxygen species
SDS = sodium dodecyl sulfate
shRNA = short hairpin RNA
SIN-1 = 3-morpholinosydnonimine
siRNA = small interfering RNA
tMCAO = transient middle cerebral artery occlusion
TUNEL = terminal deoxynucleotidyl transferase dUTP nick end labeling
ZO-1 = zonula occludens-1

Hepatitis C Virus NS3/4A Protease Inhibits Complement Activation by Cleaving Complement Component 4

Seiichi Mawatari[1], Hirofumi Uto[1*], Akio Ido[1], Kenji Nakashima[2], Tetsuro Suzuki[2], Shuji Kanmura[1], Kotaro Kumagai[1], Kohei Oda[1], Kazuaki Tabu[1], Tsutomu Tamai[1], Akihiro Moriuchi[1], Makoto Oketani[1], Yuko Shimada[3], Masayuki Sudoh[4], Ikuo Shoji[5], Hirohito Tsubouchi[6]

1 Digestive and Lifestyle Diseases, Department of Human and Environmental Sciences, Kagoshima University Graduate School of Medical and Dental Sciences, Kagoshima, Kagoshima, Japan, **2** Department of Infectious Diseases, Hamamatsu University School of Medicine, Hamamatsu, Shizuoka, Japan, **3** Miyazaki Prefectural Industrial Support Foundation, Miyazaki, Miyazaki, Japan, **4** Kamakura Research Division, Chugai Pharmaceutical, Co. Ltd., Kamakura, Kanagawa, Japan, **5** Division of Microbiology, Kobe University Graduate School of Medicine, Kobe, Japan, **6** Department of HGF Tissue Repair and Regenerative Medicine, Kagoshima University Graduate School of Medical and Dental Sciences, Kagoshima, Japan

Abstract

Background: It has been hypothesized that persistent hepatitis C virus (HCV) infection is mediated in part by viral proteins that abrogate the host immune response, including the complement system, but the precise mechanisms are not well understood. We investigated whether HCV proteins are involved in the fragmentation of complement component 4 (C4), composed of subunits C4α, C4β, and C4γ, and the role of HCV proteins in complement activation.

Methods: Human C4 was incubated with HCV nonstructural (NS) 3/4A protease, core, or NS5. Samples were separated by sodium dodecyl sulfate-polyacrylamide gel electrophoresis and then subjected to peptide sequencing. The activity of the classical complement pathway was examined using an erythrocyte hemolysis assay. The cleavage pattern of C4 in NS3/4A-expressing and HCV-infected cells, respectively, was also examined.

Results: HCV NS3/4A protease cleaved C4γ in a concentration-dependent manner, but viral core and NS5 did not. A specific inhibitor of NS3/4A protease reduced C4γ cleavage. NS3/4A protease–mediated cleavage of C4 inhibited classical pathway activation, which was abrogated by a NS3/4A protease inhibitor. In addition, co-transfection of cells with C4 and wild-type NS3/4A, but not a catalytic-site mutant of NS3/4A, produced cleaved C4γ fragments. Such C4 processing, with a concomitant reduction in levels of full-length C4γ, was also observed in HCV-infected cells expressing C4.

Conclusions: C4 is a novel cellular substrate of the HCV NS3/4A protease. Understanding disturbances in the complement system mediated by NS3/4A protease may provide new insights into the mechanisms underlying persistent HCV infection.

Citation: Mawatari S, Uto H, Ido A, Nakashima K, Suzuki T, et al. (2013) Hepatitis C Virus NS3/4A Protease Inhibits Complement Activation by Cleaving Complement Component 4. PLoS ONE 8(12): e82094. doi:10.1371/journal.pone.0082094

Editor: Ferruccio Bonino, University of Pisa, Italy

Received September 20, 2013; **Accepted** October 11, 2013; **Published** December 12, 2013

Funding: This study was supported by a Grant-in-Aid for Research on Hepatitis and BSE from the Ministry of Health, Labour and Welfare of Japan; a grant for Scientific Research from the Ministry of Education, Culture, Sports, Science and Technology of Japan; and a grant from the Miyazaki Prefecture Collaboration of Regional Entities for the Advancement of Technological Excellence. The funders had no role in study design, data collection and analysis, decision to publish, or preparation of the manuscript.

Competing interests: The authors disclose the following: M. Sudoh is employee of Chugai Pharmaceutical Co., Ltd. H. Tsubouchi holds endowed faculty position in research for HGF tissue repair and regenerative medicine, and has received funds from Eisai Co., Ltd. The remaining authors disclose no conflicts. This does not alter the authors' adherence to all the PLOS ONE policies on sharing data and materials.

* E-mail: hirouto@m2.kufm.kagoshima-u.ac.jp

Introduction

Hepatitis C virus (HCV) is a single-stranded positive-strand RNA virus of the Flaviviridae family. The viral genome encodes four structural proteins and six non-structural (NS) proteins [1]. NS3/4A, a complex consisting of NS3 with serine protease activity and cofactor NS4A, plays an essential role in processing of HCV proteins. NS3/4A is a target of direct-acting antiviral agents (DAA) [2,3], and use of an NS3/4A protease inhibitor as a DAA markedly increases the therapeutic effect of other anti-HCV agents. Thus, NS3/4A protease may play an important role in interfering with the antiviral response.

HCV has been hypothesized to block the host immune response against persistent infection [4]. Furthermore, the time required for HCV-infected patients to develop hepatic cirrhosis varies among individuals; in particular, the progression of

hepatic fibrosis seems to be slower in HCV carriers with persistent normal alanine aminotransferase (ALT) levels than in chronic hepatitis patients with elevated ALT levels [5]. These differences in clinical features might be caused by variations in the host immune response, but the underling mechanism is unclear.

In the course of proteomic analyses aimed at identifying proteins potentially involved in the pathophysiology of hepatic diseases, we found that a specific peptide fragment of complement component 4 (C4) was significantly more abundant in HCV carriers with persistent normal ALT than in patients with chronic hepatitis [6], as well as more abundant in HCV carriers, regardless of ALT levels, compared to healthy controls. Assuming that C4 expression levels are similar among these groups, this C4 fragment may be generated by post-translational processing in HCV-infected individuals.

The complement system is part of the innate immune system, which can be activated through three pathways: the classical pathway, the mannose-binding lectin pathway, and the alternative pathway. C4, which is involved in the classical- and mannose-binding lectin pathways, can be cleaved by certain cellular protease(s), leading to a cascade of C4 activation [7]. In this study, we provide the first evidence that HCV NS3/4A cleaves C4, and that this cleavage attenuates activation of the classical pathway of complement system.

Materials and Methods

Materials

HCV NS3/4A protease (217 amino acid [aa] fusion protein with NS4A co-factor fused to the N-terminus of NS3 protease domain) with His-tag, HCV core (aa 1–102) with GST-tag, and HCV NS5 (aa 2061–2302) with GST-tag were purchased from AnaSpec (Fremont, CA) or ProSpec (Rehovot, Israel). Isolated human-derived complement components (C1, C2) were obtained from Hycult Biotech (Uden, Netherlands), and C4 and C4-deficient guinea pig serum (C4d-GPS) were purchased from Sigma-Aldrich (St. Louis, MO). VX950, a HCV NS3/4A serine protease inhibitor, was obtained from Selleck Chemicals (Houston, TX). Veronal buffer, sheep erythrocytes, and hemolysin were purchased from Wako (Osaka, Japan), Nippon Biotest Laboratories Inc. (Tokyo, Japan), and Denka Seiken Co. (Tokyo, Japan), respectively.

NS3/4A protease cleavage assay

HCV NS3/4A protease, core, or NS5 (3 µl) and 9 µl of Assay buffer (SensoLyte® 490 HCV Protease Assay Kit, AnaSpec) containing 30 mM dithiothreitol (DTT) were added to C4 (3 µl), and the mixture was incubated at 30°C for 30 min. The solution was separated by sodium dodecyl sulfate polyacrylamide gel electrophoresis (SDS-PAGE), and resolved proteins were stained with Coomassie brilliant blue (CBB). In a separate experiment, VX950 was pre-incubated with NS3/4A protease at 30°C for 30 min, and then incubated with C4 at 30°C for 30 min. Proteins detected by CBB staining were subjected to N-terminal peptide sequence analysis at Nippi Inc. (Tokyo, Japan).

Hemolytic analysis

The method used for hemolytic analysis has been described previously [8,9]. Briefly, intermediates of complement components were sequentially added to sheep erythrocytes sensitized by hemolysin (Ab-sensitized sheep erythrocytes, EA). Dilute erythrocytes and complement components were prepared in Veronal buffer containing 2% gelatin (GVB). To prepare EA, hemolysin was added to 10 ml of erythrocytes (5×10^8 cells/ml) and incubated at 37°C for 30 min. C1 (10 µg) was added to 5 ml of EA, incubated at 30°C for 15 min, and washed twice with GVB (EAC1). NS3/4A protease was prepared in a solution containing 20 mM Tris-HCl (pH 8.0), 20% glycerol, 100 mM KCl, 1 mM DTT, and 0.2 mM EDTA, adjusted to pH 7.5. The reaction solution was adjusted to 2 mM DTT to ensure a uniform effect on C4 activity. C4 was incubated with the NS3/4A protease, and then mixed with 100 µl of EAC1 and incubated at 30°C for 15 min (EAC1-C4). After washing twice with GVB, 1 µl of C2 (0.1 mg/ml) was added and the mixture was incubated at room temperature for 4 min (EAC1-C4-C2). After washing twice again with GVB, 150 µl of 80-fold diluted C4d-GPS was added to 30 µl of EAC1-C4-C2, and the mixture was incubated at 37°C for 30 min. The optical absorbance of the centrifuged supernatant was determined at 415 nm, and the level of hemolysis was calculated using the following formula: Hemolysis (%) = (sample OD_{415} – no C4 OD_{415})/(total hemolysis in distilled water OD_{415} – no C4 OD_{415}) ×100. "No C4" refers to a control sample containing EAC1 not incubated with C4. In a separate experiment, VX950 was first pre-incubated with NS3/4A protease at 30°C for 30 min, and then incubated with C4 at 30°C for 30 min.

Cell culture and transfection

Human hepatoma-derived Huh7.5.1 cells (a kind gift from Dr. F. V. Chisari, The Scripps Research Institute, La Jolla, CA) and human embryonic kidney (HEK) 293T cells were cultured at 37°C under 5% CO_2 in DMEM containing 10% FBS, 100 units/ml penicillin, and 100 g/ml streptomycin. DNA transfections of Huh7.5.1 cells and 293T cells were performed using Lipofectamine LTX/PLUS Reagent (Invitrogen, Carlsbad, CA) and polyethylenimine (Alfa Aesar, Heysham, Lancashire, UK), respectively. The transfection complex was formed at a DNA:reagent ratio of 1:1 (w/w) in OptiMEM (Invitrogen) with incubation for 15 min at room temperature before it was added to the culture.

Preparation of virus stock

The pJ6/JFH1 plasmid was generated by replacing the structural region of the JFH-1 strain with that of the J6CF strain, as described [10]. Cell culture–derived infectious HCV particles (HCVcc) were produced by introducing *in vitro* transcribed RNA from pJ6/JFH1 into Huh-7.5.1 cells by electroporation. The culture supernatant was concentrated using a 100-kDa MWCO Amicon Ultra Centrifugal Filter (Millipore, Bedford, MA). Virus infectivity was measured by indirect immunofluorescence analysis. Virus stocks (1×10^7 focus-forming units/ml) were divided into small aliquots and stored at −80 °C until use.

Plasmids

The C4 expression plasmid pFN21-C4A was purchased from Kazusa DNA Research Institute (Kisarazu, Japan). To create pFN21-C4A delH-Tag, the N-terminal Halo-Tag of pFN21-C4A was removed by digestion with *Hin*dIII and *Pvu*I, followed by blunt-ending with KOD FX neo (Toyobo, Osaka, Japan). pCAG-HA-NS3/4A, which expresses full-length NS3 and NS4 (derived from HCV genotype 1b, Con-1 strain) with an HA tag at the N-terminus of NS3 was generated as described [11]. Point mutation of serine to alanine at position 139 (S139A) in pCAG-HA-NS3/4A was achieved by site-directed mutagenesis using two primers: 5′-TAC TTG AAG GGC TCT GCG GGC GGT CCA CTG C-3′ and 5′-GCA GTG GAC CGC CCG CAG AGC CCT TCA AGT A-3′. The point mutation was confirmed by DNA sequencing.

Immunoprecipitation and immunoblotting

Goat anti-human complement C4 antibody (MP Biomedicals, Santa Ana, CA) was bound to protein G–agarose beads (Thermo Scientific, Rockford, IL) in binding buffer (0.5% Nonidet P-40, 25 mM Tris [pH 7.5], 150 mM NaCl, 1 mM EDTA and protease inhibitor cocktail [Roche, Basel, Switzerland]) for 1 h at room temperature. Culture supernatants were incubated with the beads for 1 h at room temperature, and the immunoprecipitated proteins were eluted by heat treatment for 5 min at 100°C with 2× sample buffer. Culture supernatants were directly mixed with 3× sample buffer at a ratio of 1 volume supernatant to 2 volumes sample buffer (1:2 [v/v]). Cells were solubilized in lysis buffer (1% Triton X-100, 25 mM Tris, pH 7.5, 150 mM NaCl, 1 mM EDTA and protease inhibitor cocktail) on ice. Cell debris was removed by centrifugation, and the resultant supernatants were diluted 1:2 (v/v) with 3× sample buffer. Precipitated proteins, culture supernatants, and cell lysates were separated by SDS-PAGE and transferred to polyvinylidene difluoride (PVDF) membranes (Immobilon-P, Millipore). After blocking in 4% BlockAce (DS Pharma Biomedical, Osaka, Japan), the blots were incubated with the indicated primary antibodies, followed by the secondary antibody in TBST (25 mM Tris [pH 7.5], 150 mM NaCl, and 0.1% Tween 20). The primary antibodies used were anti-C4γ (clone H-291, Santa Cruz Biotechnology, Dallas, TX), anti-human complement C4, anti-HA (Sigma, St. Louis, MO), anti-HCV core (clone 2H9) and anti-GAPDH (clone 6C5, Santa Cruz Biotechnology). Donkey polyclonal Secondary Antibody to Goat IgG-H&L (HRP) (Abcam, Cambridge, UK), HRP-linked anti-mouse IgG, and HRP-linked anti–rabbit IgG (Cell Signaling Technology, Danvers, MA) were used as secondary antibodies. Finally, proteins were visualized using an enhanced chemiluminescence (ECL) reagent (ECL Select Western Blotting Detection Reagent, GE Healthcare, Little Chalfont, UK).

Statistical analysis

The concentration of proteins detected by Western blots was determined by densitometric analysis using the ImageJ software [12]. Statistical analysis was performed with the SPSS software (SPSS Inc., Chicago, IL) using the Tukey test, with $P < 0.05$ considered to indicate a significant difference.

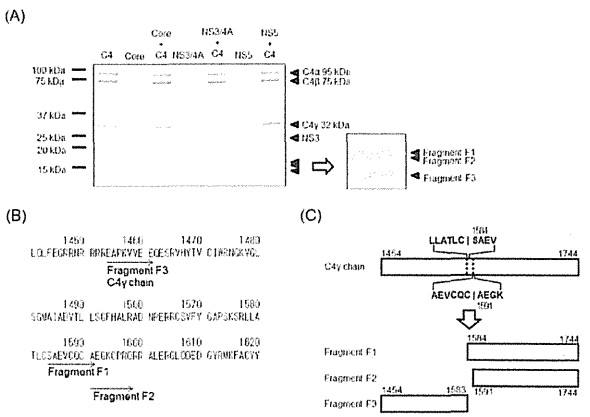

Figure 1. C4 is cleaved by HCV NS3/4A protease at Cys-1583/Ser-1584 or Cys-1590/Ala-1591. (A) HCV NS3/4A protease, core, or NS5 was added to C4, and the products were separated by SDS-PAGE and subjected to CBB staining. Two approximately 17-kDa proteins (Fragment F1 and F2) and a 15-kDa protein (Fragment F3) were detected after incubation of C4 with HCV NS3/4A protease, but not after incubation with core or NS5. (B) Amino acid sequence of aa 1451-1620 region of C4. Protein fragments were analyzed by N-terminal peptide sequencing. The sequences of the N-termini of the 17-kDa proteins (Fragment F1 and F2) were SAEVCQCA and AEGKCPRQ, which are located at aa 1584–1591 and 1591–1598 in C4, respectively. The sequence of the N-terminus of the 15-kDa protein (Fragment F3) was EAPKVVEE, which is located at aa 1454–1461 in C4. (C) Schematic representation of C4γ chain, and Fragment F1, F2 and F3.

doi: 10.1371/journal.pone.0082094.g001

Results

HCV NS3/4A protease cleaves C4 in vitro

To test cleavage of C4 mediated by HCV proteins, C4 (containing subunits C4α, C4β, and C4γ) was mixed with NS3/4A protease, core, or NS5, followed by incubation at 30°C for 30 min. As shown in Figure 1A, doublet bands at 17 kDa (fragments F1 and F2 in the enlarged view) and one band at 15 kDa (fragment F3) were detected in the presence of NS3/4A protease and C4. These bands were not detected after incubation of C4 with core or NS5, or when either core or NS5 were incubated alone.

N-terminal sequence analyses revealed that the bands at approximately 100, 75, and 32 kDa (Figure 1A) represented C4α (N-terminus sequence identified: NVNFQKAI), C4β (KPRLLLFS), and C4γ (EAPKVVEE), respectively. As shown in Figure 1B, the N-terminal sequences of the doublet proteins at 17 kDa were identical to sequences found in C4γ: SAEVCQCA (aa 1584–1591 of C4) and AEGKCPRQ (aa 1591–1598). In addition, the N-terminal sequence of the 15-kDa fragment was EAPKVVEE (aa 1454–1461), indicating that the 15-kDa fragment is the N-terminal region of the C4γ. These results demonstrate that HCV NS3/4A protease cleaves C4 between

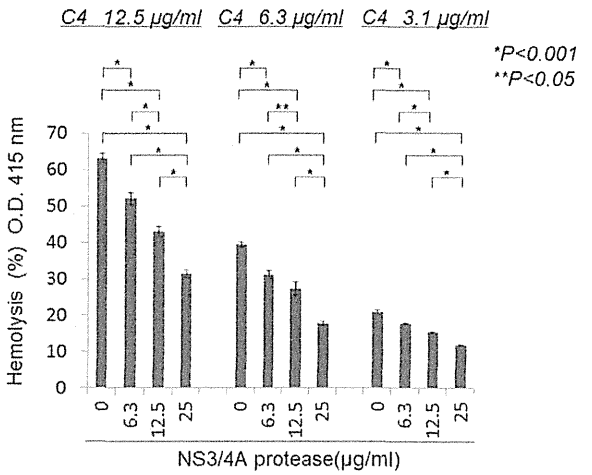

Figure 2. HCV NS3/4A protease inhibits the classical pathway, as assessed by hemolysis. C4 was incubated in the presence or absence of HCV NS3/4A protease, and then C1-sensitized EA (EAC1) was added (EAC1-C4). After washing, C2 was added to form EAC1-C4-C2, and the complex was resuspended in C4d-GPS. The absorbance of the centrifuged supernatant was determined at 415 nm. The grade of hemolysis decreased in the presence of NS3/4A protease in a dose-dependent manner. All measurements were performed in triplicate, and data are expressed as means ± SD.

doi: 10.1371/journal.pone.0082094.g002

either Cys-1583 and Ser-1584 or Cys-1590 and Ala-1591, consistent with the consensus sequence of HCV NS3 proteinase cleavage sites [3,13]. Possible locations for the 15- and 17-kDa fragments of C4γ are shown in Figure 1B and 1C.

HCV NS3/4A protease decreases the activity of the classical pathway of the complement system in a concentration-dependent manner

To examine the functional significance of C4 cleavage by NS3/4A protease, complement components were serially added to EA to reproduce the classical pathway of the complement system. C4, untreated or treated with various concentrations of NS3/4A, was added at various concentrations to the EA-C1 mixture, followed by addition of C2 and C4d-GPS, which were used as sources of C3 and C5-C9. Erythrocyte hemolysis, which is caused by the complement-mediated fusion of erythrocytes, was quantified (Figure 2). NS3/4A treatment significantly decreased hemolysis levels in a concentration-dependent manner. This result, together with those in Figure 1, suggests that the C4 cleavage mediated by NS3/4A protease may contribute to inhibition of complement activation via the classical pathway.

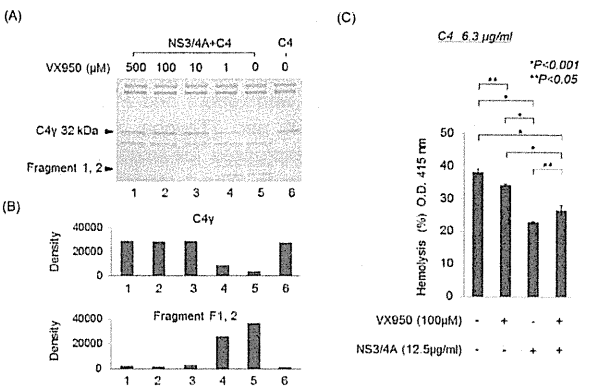

Figure 3. VX950, a HCV NS3/4A protease inhibitor, abrogates cleavage of C4 induced by HCV NS3/4A protease. (A) VX950 was added to HCV NS3/4A protease at the indicated concentrations, and then C4 was added. Proteins were separated by SDS-PAGE for CBB staining. The three C4-derived fragments of 17 kDa and 15 kDa produced by NS3/4A protease action could not be detected after pretreatment with VX950, and this change was accompanied by an increased concentration of the 32-kDa C4γ chain. (B) The C4γ, 17-kDa, and 15-kDa bands were quantified by densitometric analysis using the Image J software. (C) C4 was incubated in the presence or absence of HCV NS3/4A or VX950, and then C1-sensitized EA (EAC1) was added (EAC1–C4). C2 and C4d-GPS were then added, and the absorbance of the supernatant was determined at 415 nm. Hemolysis was inhibited by NS3/4A protease and this inhibition was blocked by VX950. All measurements were made in triplicate, and data are expressed as means ± SD.

doi: 10.1371/journal.pone.0082094.g003

HCV protease inhibitor reduces inactivation of complement by blocking C4 cleavage by NS3/4A protease

We tested the effect of VX950, a specific inhibitor of NS3/4A protease, on C4 cleavage by NS3/4A protease and inhibition of complement activation. As shown in Figure 3A and 3B, under a condition in which more than 80% of 32-kDa C4γ was processed into 17- and 15-kDa fragments in the presence of NS3/4A protease (lanes 5), pretreatment of the protease with 1 μM VX950 moderately inhibited the cleavage of C4γ (lanes 4). The NS3/4A-mediated processing of C4γ into 17- and 15-kDa fragments was almost completely blocked by VX950 at ≥10 μM (lanes 1–3). In the erythrocyte hemolysis assay, the reduction in hemolysis level mediated by NS3/4A significantly recovered in the presence of VX950 (Figure 3C). These results confirmed cleavage of C4γ by NS3/4A and the involvement of the protease in the classical complement pathway.

Cleavage of C4γ in NS3/4A-expressing cells and HCV-infected cells

To determine whether HCV NS3/4A protease cleaves C4 in cells, we analyzed 32-kDa C4γ and its processed fragments in

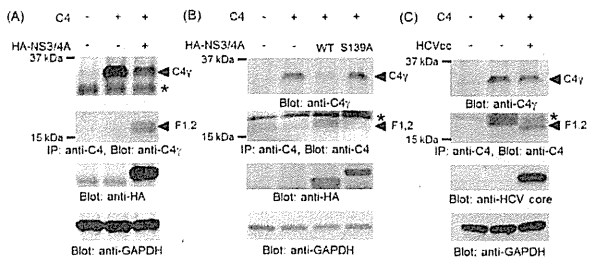

Figure 4. C4 is cleaved by HCV NS3/4 protease in cell cultures. (A) 293T cells were transfected with the indicated plasmids. Anti-C4 immunoprecipitates (IP) of supernatants were separated by SDS-PAGE and analyzed by immunoblotting with anti-C4γ antibody. Detergent-soluble cell lysates were separated by SDS-PAGE and analyzed by immunoblotting with anti-HA and anti-GAPDH antibodies. (B) 293T cells were transfected with the indicated plasmids. Culture supernatants were analyzed by immunoblotting with anti-C4γ antibody. Anti-C4 immunoprecipitates (IP) of supernatants were analyzed by immunoblotting with anti-C4 antibody. Detergent-soluble cell lysates were analyzed by immunoblotting with anti-HA and anti-GAPDH antibodies. (C) Huh7.5.1 cells were mock-infected or infected with HCVcc at a multiplicity of infection of 2 for 6 h, followed by mock-transfection or transfection with C4 expression plasmid. Culture supernatants and cell lysates were analyzed as described in (A) and (B). The anti-C4γ antibody was not appropriate for immunoblotting of IP samples derived from Huh7.5.1 cultures because of unavoidable nonspecific cross-reaction. * indicates non-specific reactions in (A) – (C).

doi: 10.1371/journal.pone.0082094.g004

culture medium from 293T cells cotransfected with expression plasmids encoding C4 (pFN21-C4A delH-Tag) and NS3/4A protease (pCAG-HA-NS3/4A). Co-expression of C4 and NS3/4A derived from HCV genotype 1b led to production of the 17-kDa C4γ fragment and reduction in the level of 32-kDa C4γ (Figure 4A). In contrast, the 17-kDa fragment was not detected, and the 32-kDa C4γ level was not changed, when a mutant NS3 with an amino-acid substitution at the catalytic-site (S139A)/4A was co-expressed with C4 (Figure 4B). Next, we investigated C4 cleavage in HCV-infected cultures. In the culture medium of Huh7.5.1 cells infected with HCVcc of strain J6/JFH-1 (genotype 2a) expressing of C4 from pFN21-C4A delH-Tag, the 17-kDa fragment was produced, and the level of 32-kDa C4γ was reduced accordingly (Figure 4C). These data demonstrate that C4γ can be cleaved by HCV NS3/4A, either expressed from a plasmid or in HCV-infected cells, and that proteases of both genotypes 1b and 2a are functional in this cleavage.

Discussion

The results of this study show that C4γ is cleaved by HCV NS3/4A protease *in vitro* and in cell culture. Cleavage of C4 by HCV NS3/4A protease leads to inhibition of activity of the classical complement pathway. C4 cleavage and abrogation of complement activation are blocked by an inhibitor of NS3/4A protease.

HCV NS3/4A protease plays an important role in the replication of non-structural regions [2,3], and might also directly act on the IFN signaling system to inhibit the host immune response and prevent viral clearance, thereby contributing to persistent HCV infection. However, a direct relationship between HCV infection and complement components has not been previously established. Levels of functional C3 or C4 assessed by hemolysis assay are reduced after infection by flaviviruses such as Dengue virus and West Nile virus (WNV) [9,14]. In mice infected with γ-herpesvirus or WNV, genetic deletion of complement C3 or C4 not only enhances mortality but also increases persistent replication of γ-herpesvirus or WNW RNA levels [14,15]. Furthermore, Moulton et al. reported that mousepox virus dissemination was more severe, and viral loads in tissues were higher, in C3-deficient mice; leading to higher mortality than in wild-type mice; those authors concluded that the complement system is critical for slowing viral spread and decreasing tissue titer and damage [16]. Thus, it is likely that the complement system is widely associated with development of viral infection. Further investigation of the role of complement activation mediated by HCV proteins such as HCV NS3/4A protease may provide new insights into development of persistent HCV infection.

Our results indicated that the C4 cleavage site of HCV NS3/4A protease is between either Cys-1583 and Ser-1584 or Cys-1590 and Ala-1591 of C4, both of which are located in the C4γ chain (Figure 1). HCV NS3/4A protease has previously been suggested to cleave at Cys/Thr and Ala/Ser sites [3,13], which is broadly consistent with our results. C4 was also cleaved by HCV NS3/4A protease in HCV-infected cells (Figure 4C), in which unprocessed 32-kDa C4γ and cleaved 17-kDa fragment in the culture medium were observed. In cultures of human hepatoma HepG2 cells, the major fraction of C4α, C4β, and C4γ were present in the culture medium rather than in cells [17,18]. In good agreement with that finding, we detected little C4 in Huh-7–derived cells (data not shown). We speculate that immediately after synthesis, at least a fraction of C4γ can be quickly cleaved by NS3/4A in virally replicating cells, followed by secretion into the culture medium. However, we cannot rule out the possibility that HCV NS3/4A protease is present extracellularly and is functional under some particular conditions, because addition of recombinant antigens derived from the NS3 region to NS4 improves the sensitivity of the anti-HCV test in serum and shortens the window period for seroconversion in patients infected with HCV [19].

Complement components are involved in innate immunity and are responsible for one of the major immunological mechanisms mediated by antibodies [7]. In viral and bacterial infection, these components cause lysis of the outer membrane of virus particles [20] and infected cells [21] by the membrane attack complex C5–C9, ultimately resulting in elimination of the pathogen. Some viruses, such as cytomegalovirus, induce expression of cellular complement inhibitors, for example, decay-accelerating factor and monocyte chemoattractant protein, leading to increased levels of these proteins on the

surfaces of infected cells. Human immunodeficiency virus may incorporate the complement inhibitors into the viral envelope [22,23]. NS1 protein secreted from flaviviruses, such as dengue virus, West Nile virus, and yellow fever virus, not only attenuates activation of the classical and lectin pathways by directly interacting with C4, but also inactivates C4b by interacting with C4-binding protein [9,24]. Thus, NS1 of flaviviruses is considered to play a role in protecting the virus from complement-dependent neutralization. To our knowledge, however, our study provides the first evidence that the viral protease plays a role in protecting the virus from the complement defense system via proteolytic processing of the complement component.

In particular, C4 is involved in the classical and mannose-binding lectin pathways of the complement system, and it is responsible for the major activity of complement components. Upon antibody binding to an antigen, C4 is cleaved into C4a and C4b by the C1q-C1r-C1s complex, and C4b then binds to C2a (C4b2a) on the cell membrane to cleave C3 into C3a and C3b. Subsequently, C3b binds to C4b2a to cleave C5, and finally C5b and C6-C9 form the membrane attack complex to cause lysis of the cell membrane [7]. The erythrocyte hemolysis assay used in this study reproduces this cascade and revealed that HCV NS3/4A protease cleaves C4 and decreases the activity of the classical pathway. The specific assay was constructed to evaluate the function of C4 in the classical pathway by allowing HCV NS3/4A protease to act on C4 alone, without influence from other complement components. Therefore, further work is needed to determine whether HCV NS3/4A protease affects other components.

Several studies have demonstrated that HCV proteins influence complement systems and may be involved in evading antiviral immune responses of the host, as follows. Amet et al. reported that CD59, which may inhibit formation of the membrane attack complex, is incorporated into cultured cells and plasma primary HCV virions and inhibited activation of complement components, whereas administration of a CD59 inhibitor increases the sensitivity of component activation against endogenous HCV viral particles [25]. Banerjee et al. found that the HCV core protein reduces the expression of upstream stimulatory factor (USF)-1, a transcription factor important for basal C4 expression, and that expression of interferon regulatory factor (IRF)-1, which is important for IFN-γ–induced C4 expression, is inhibited by hepatocytes expressing HCV NS5A [26]. Mazumdar et al. showed that NS5A strongly downregulates C3 promoter activity in the presence of IL-1β, acting as an inducer [27]. HCV core inhibits T-cell proliferative responses *in vitro*, and this effect can be reversed by addition of anti–C1q receptor antibody to a T-cell proliferation assay [28]. Here, we identified C4γ as a novel cellular substrate of the HCV NS3/4A protease.

The results of this study suggest that C4γ cleavage by NS3/4A decreased the activity of the classical complement pathway, and might thereby attenuate activation of the complement system. An understanding of the viral protease–mediated inhibition of the complement system should provide new insights into the roles played by immune evasion in persistent HCV infection.

Acknowledgements

We wish to thank the Joint Research Laboratory, Kagoshima University Graduate School of Medical and Dental Sciences, for the use of their facilities.

Author Contributions

Conceived and designed the experiments: SM HU YS MS HT. Performed the experiments: SM KN TS SK KK KO KT TT AM MO. Analyzed the data: SM HU AI KN TS YS. Contributed reagents/materials/analysis tools: HU IS HT. Wrote the manuscript: SM HU TS HT.

References

1. Rehermann B (2009) Hepatitis C virus versus innate and adaptive immune responses: a tale of coevolution and coexistence. J Clin Invest 119: 1745-1754. doi:10.1172/JCI39133. PubMed: 19587449.
2. Moradpour D, Penin F, Rice CM (2007) Replication of hepatitis C virus. Nat Rev Microbiol 5: 453-463. doi:10.1038/nrmicro1645. PubMed: 17487147.
3. Morikawa K, Lange CM, Gouttenoire J, Meylan E, Brass V et al. (2011) Nonstructural protein 3-4A: the Swiss army knife of hepatitis C virus. J Viral Hepat 18: 305-315. doi:10.1111/j.1365-2893.2011.01451.x. PubMed: 21470343.
4. Barnaba V (2010) Hepatitis C virus infection: a "liaison a trois" amongst the virus, the host, and chronic low-level inflammation for human survival. J Hepatol 53: 752-761. doi:10.1016/j.jhep.2010.06.003. PubMed: 20673595.
5. Persico M, Perrotta S, Persico E, Terracciano L, Folgori A et al. (2006) Hepatitis C virus carriers with persistently normal ALT levels: biological peculiarities and update of the natural history of liver disease at 10 years. J Viral Hepat 13: 290-296. doi:10.1111/j.1365-2893.2005.00667.x. PubMed: 16637858.
6. Imakiire K, Uto H, Sato Y, Sasaki F, Mawatari S et al. (2012) Difference in serum complement component C4a levels between hepatitis C virus carriers with persistently normal alanine aminotransferase levels or chronic hepatitis C. Mol Med Rep 6: 259-264. PubMed: 22614103.
7. Walport MJ (2001) Complement. First of two parts. N Engl J Med 344: 1058-1066. doi:10.1056/NEJM200104053441406. PubMed: 11287977.
8. Krych-Goldberg M, Hauhart RE, Subramanian VB, Yurcisin BM 2nd, Crimmins DL et al. (1999) Decay accelerating activity of complement receptor type 1 (CD35). Two active sites are required for dissociating C5 convertases. J Biol Chem 274: 31160-31168. doi:10.1074/jbc.274.44.31160. PubMed: 10531307.
9. Avirutnan P, Fuchs A, Hauhart RE, Somnuke P, Youn S et al. (2010) Antagonism of the complement component C4 by flavivirus nonstructural protein NS1. J Exp Med 207: 793-806. doi:10.1084/jem.20092545. PubMed: 20308361.
10. Murayama A, Weng L, Date T, Akazawa D, Tian X et al. (2010) RNA polymerase activity and specific RNA structure are required for efficient HCV replication in cultured cells. PLoS Pathog 6:e1000885. PubMed: 20442786.
11. Matsui C, Shoji I, Kaneda S, Sianipar IR, Deng L et al. (2012) Hepatitis C virus infection suppresses GLUT2 gene expression via downregulation of hepatocyte nuclear factor 1α. J Virol 86: 12903-12911. doi:10.1128/JVI.01418-12. PubMed: 22993150.
12. Schneider CA, Rasband WS, Eliceiri KW (2012) NIH Image to ImageJ: 25 years of image analysis. Nat Methods 9: 671-675. doi:10.1038/nmeth.2089. PubMed: 22930834.
13. Bartenschlager R, Ahlborn-Laake L, Yasargil K, Mous J, Jacobsen H (1995) Substrate determinants for cleavage in cis and in trans by the hepatitis C virus NS3 proteinase. J Virol 69: 198-205. PubMed: 7983710.
14. Mehlhop E, Diamond MS (2006) Protective immune responses against West Nile virus are primed by distinct complement activation pathways.

J Exp Med 203: 1371-1381. doi:10.1084/jem.20052388. PubMed: 16651386.
15. Kapadia SB, Levine B, Speck SH, Virgin HW 4th (2002) Critical role of complement and viral evasion of complement in acute, persistent, and latent gamma-herpesvirus infection. Immunity 17: 143-155. doi: 10.1016/S1074-7613(02)00369-2. PubMed: 12196286.
16. Moulton EA, Atkinson JP, Buller RM (2008) Surviving mousepox infection requires the complement system. PLoS Pathog 4:e1000249. PubMed: 19112490.
17. Chan AC, Atkinson JP (1983) Identification and structural characterization of two incompletely processed forms of the fourth component of human complement. J Clin Invest 72: 1639-1649. doi: 10.1172/JCI111123. PubMed: 6313766.
18. Andoh A, Fujiyama Y, Bamba T, Hosoda S (1993) Differential cytokine regulation of complement C3, C4, and factor B synthesis in human intestinal epithelial cell line, Caco-2. J Immunol 151: 4239-4247. PubMed: 8409399.
19. Mattsson L, Gutierrez RA, Dawson GJ, Lesniewski RR, Mushahwar LK et al. (1991) Antibodies to recombinant and synthetic peptides derived from the hepatitis C virus genome in long-term-studied patients with posttransfusion hepatitis C. Scand J Gastroenterol 26: 1257-1262. doi: 10.3109/00365529108998622. PubMed: 1722348.
20. Sullivan BL, Knopoff EJ, Saifuddin M, Takefman DM, Saarloos MN et al. (1996) Susceptibility of HIV-1 plasma virus to complement-mediated lysis. Evidence for a role in clearance of virus in vivo. J Immunol 157: 1791-1798. PubMed: 8759769.
21. Terajima M, Cruz J, Co MD, Lee JH, Kaur K et al. (2011) Complement-dependent lysis of influenza a virus-infected cells by broadly cross-reactive human monoclonal antibodies. J Virol 85: 13463-13467. doi: 10.1128/JVI.05193-11. PubMed: 21994454.
22. Blom AM (2004) Strategies developed by bacteria and virus for protection from the human complement system. Scand J Clin Lab Invest 64: 479-496. doi:10.1080/00365510410002904. PubMed: 15276914.
23. Finlay BB, McFadden G (2006) Anti-immunology: evasion of the host immune system by bacterial and viral pathogens. Cell 124: 767-782. doi:10.1016/j.cell.2006.01.034. PubMed: 16497587.
24. Avirutnan P, Hauhart RE, Somnuke P, Blom AM, Diamond MS et al. (2011) Binding of flavivirus nonstructural protein NS1 to C4b binding protein modulates complement activation. J Immunol 187: 424-433. doi: 10.4049/jimmunol.1100750. PubMed: 21642539.
25. Amet T, Ghabril M, Chalasani N, Byrd D, Hu N et al. (2012) CD59 incorporation protects hepatitis C virus against complement-mediated destruction. Hepatology 55: 354-363. doi:10.1002/hep.24686. PubMed: 21932413.
26. Banerjee A, Mazumdar B, Meyer K, Di Bisceglie AM, Ray RB et al. (2011) Transcriptional repression of C4 complement by hepatitis C virus proteins. J Virol 85: 4157-4166. doi:10.1128/JVI.02449-10. PubMed: 21345967.
27. Mazumdar B, Kim H, Meyer K, Bose SK, Di Bisceglie AM et al. (2012) Hepatitis C virus proteins inhibit C3 complement production. J Virol 86: 2221-2228. doi:10.1128/JVI.06577-11. PubMed: 22171262.
28. Kittlesen DJ, Chianese-Bullock KA, Yao ZQ, Braciale TJ, Hahn YS (2000) Interaction between complement receptor gC1qR and hepatitis C virus core protein inhibits T-lymphocyte proliferation. J Clin Invest 106: 1239-1249. doi:10.1172/JCI10323. PubMed: 11086025.

VIROLOGY JOURNAL

RESEARCH Open Access

Antiviral activities of Indonesian medicinal plants in the East Java region against hepatitis C virus

Tutik Sri Wahyuni[1,3], Lydia Tumewu[2], Adita Ayu Permanasari[2], Evhy Apriani[2], Myrna Adianti[2,3], Abdul Rahman[1], Aty Widyawaruyanti[1], Maria Inge Lusida[2], Achmad Fuad[1], Soetjipto[2], Nasronudin[2], Hiroyuki Fuchino[4], Nobuo Kawahara[4], Ikuo Shoji[3], Lin Deng[3], Chie Aoki[3,5] and Hak Hotta[3*]

Abstract

Background: Hepatitis C virus (HCV) is a major cause of liver disease and a potential cause of substantial morbidity and mortality worldwide. The overall prevalence of HCV infection is 2%, representing 120 million people worldwide. Current standard treatment using pegylated interferon and ribavirin is effective in only 50% of the patients infected with HCV genotype 1, and is associated with significant side effects. Therefore, it is still of importance to develop new drugs for treatment of HCV. Antiviral substances obtained from natural products, including medicinal plants, are potentially good targets to study. In this study, we evaluated Indonesian medicinal plants for their anti-HCV activities.

Methods: Ethanol extracts of 21 samples derived from 17 species of medicinal plants explored in the East Java region were tested. Anti-HCV activities were determined by a cell culture method using Huh7.5 cells and HCV strains of 9 different genotypes (1a to 7a, 1b and 2b).

Results: Four of the 21 samples tested showed antiviral activities against HCV: *Toona sureni* leaves (TSL) with 50% inhibitory concentrations (IC_{50}) of 13.9 and 2.0 μg/ml against the HCV J6/JFH1-P47 and -P1 strains, respectively, *Melicope latifolia* leaves (MLL) with IC_{50} of 3.5 and 2.1 μg/ml, respectively, *Melanolepis multiglandulosa* stem (MMS) with IC_{50} of 17.1 and 6.2 μg/ml, respectively, and *Ficus fistulosa* leaves (FFL) with IC_{50} of 15.0 and 5.7 μg/ml, respectively. Time-of-addition experiments revealed that TSL and MLL inhibited both at the entry and post-entry steps while MMS and FFL principally at the entry step. TSL and MLL inhibited all of 11 HCV strains of all the genotypes tested to the same extent. On the other hand, FFL showed significantly weaker inhibitory activities against the HCV genotype 1a strain, and MMS against the HCV strains of genotypes 2b and 7a to a lesser extent, compared to the other HCV genotypes.

Conclusions: Ethanol extracts of TSL, MLL, MMS and FFL showed antiviral activities against all the HCV genotypes tested with the exception that some genotype(s) showed significant resistance to FFL and to MMS to a lesser extent. These plant extracts may be good candidates for the development of anti-HCV drugs.

Keywords: Hepatitis C virus, HCV, Antiviral activity, Medicinal plants, Indonesia, Entry inhibition

* Correspondence: hotta@kobe-u.ac.jp
[3]Division of Microbiology, Kobe University Graduate School of Medicine, Kobe, Japan
Full list of author information is available at the end of the article

Background

Hepatitis C virus (HCV) is an enveloped virus that belongs to the *Hepacivirus* genus within the *Flaviviridae* family. The viral genome is a single-stranded, positive-sense RNA of 9.6 kb with highly structured 5'- and 3'-untranslated regions [1]. It encodes a polyprotein precursor consisting of about 3,000 amino acid residues, which is cleaved by the host and viral proteases to generate 10 mature proteins, such as core, E1, E2, a putative ion channel p7, and nonstructural proteins NS2, NS3, NS4A, NS4B, NS5A and NS5B [1,2]. Core, E1 and E2 together with the viral genome form the infectious virus particle while the other nonstructural proteins are essential for viral RNA replication. The HCV genome exhibits a considerable degree of sequence heterogeneity, based on which HCV is currently classified into 7 genotypes (1 to 7) and more than 70 subtypes (1a, 1b, 2a, 2b, etc.) [3].

HCV is a major cause of chronic liver disease, such as hepatitis, liver cirrhosis and hepatocellular carcinoma, and is a potential cause of substantial morbidity and mortality [4,5]. The most recent estimate of the prevalence of HCV infection reported by the World Health Organization is 2%, representing 120 million people worldwide. A current standard treatment using pegylated interferon and ribavirin is effective in only ca. 50% of the patients infected with HCV genotype 1, and is associated with significant side effects and viral resistance [3]. Although a number of novel antivirals against HCV for clinical use are being tested, it is still of importance to develop complementary and/or alternative drugs for treatment of HCV infection from clinical and economical points of view. In this regard, antiviral substances obtained from natural products, including medicinal plants, are potentially good targets to study [6].

It is well known that certain medicinal plants possess antiviral activities. A wide variety of active phytochemicals, such as flavonoids, terpenoids, lignins, sulphides, polyphenolics, coumarins, saponins, furyl compounds, alkaloids, polylines, thiophenes, proteins and peptides, have been identified to inhibit various viruses [7]. Herbal extracts of *Boswellia carterii, Embelia schimperi, Piper cubeba, Quercus infectoria, Tranchyspermum ammi* and *Syzygium aromaticum* were shown to inhibit HCV protease activities *in vitro* [8]. A methanol extract of *Swietenia macrophilla* stem and a purified compound, 3-hydroxy caruilignan, inhibited HCV RNA replication

Table 1 Antiviral activity (IC_{50}) against HCV J6/JFH1-P47, cytotoxicity (CC_{50}) and selectivity index (SI) of Indonesian medicinal plants tested in this study

No.	Botanical name	Parts	Family	IC_{50} [a] (μg/ml)	CC_{50} (μg/ml)	SI
1.	*Eupatorium inulifolium*	Stems	Asteraceae	> 500	>500	na[b]
2.	*Calliandra polytirsa*	Leaves	Fabaceae	31.9 ± 7.1	>100	>3.1
3.	*Strophacantus membranifolius*	Herbs	Acantaceae	>100	>500	na
4.	*Cestrum calysinum*	Leaves	Solanaceae	52.1 ± 5.7	>500	>9.6
5.	*Cestrum calysinum*	Stems	Solanaceae	>500	>500	na
6.	*Eucalyptus globulus*	Stems	Myrtaceae	43.0 ± 39.5	>100	>2.3
7.	***Toona sureni*[c]**	Leaves	Meliaceae	**13.9 ± 1.6**	**> 500**	**>35.9**
8.	***Melicope latifolia*[c]**	Leaves	Rutaceae	**3.5 ± 1.4**	**>100**	**>28.6**
9.	*Melicope latifolia*	Stems	Rutaceae	42.6 ± 37.6	>100	>2.4
10.	*Piper sulcatum*	Stems	Piperaceae	38.0 ± 4.2	>100	>2.6
11.	*Fagraea blumei*	Stems	Fagaceae	>100	>500	na
12.	*Fraxinus griffithii*	Stems	Meliaceae	>500	>500	na
13.	*Maesa latifolia*	Leaves	Myrsinaceae	32.7 ± 6.6	>100	>3.1
14.	*Maesa latifolia*	Stems	Myrsinaceae	32.2 ± 10.2	>100	>3.1
15.	***Melanolepis multiglandulosa*[c]**	Stems	Euphorbiaceae	**17.1 ± 1.6**	**>100**	**>5.8**
16.	*Acacia decurens*	Leaves	Fabaceae	44.9 ± 7.1	>500	>11.1
17.	*Randia maculata*	Stems	Rubiaceae	38.7 ± 5.7	>500	>12.9
18.	*Gompostemma polythirsa*	Flowers	Acanthaceae	92.8 ± 19.8	>500	>5.4
19.	*Acmena acuminatissima*	Leaves	Myrtaceae	>100	>100	na
20.	*Acmena acuminatissima*	Stems	Myrtaceae	>100	>500	na
21.	***Ficus fistulosa*[c]**	Leaves	Moraceae	**15.0 ± 7.1**	**>100**	**>7.6**

[a]Data represent means ± SEM of data from two independent experiments using HCV J6/JFH1-P47.
[b]Not applicable.
[c]The plant extracts with IC_{50} of <20 μg/ml and CC_{50} of >100 μg/ml are written in boldface letters.

in Huh7 cells harboring an HCV subgenomic RNA replicon [9]. Also, inhibition of HCV replication by herbal extracts was reported on leaves and roots of *Phyllantus amarus* (Euphorbiaceae) [10]. Moreover, a number of bioflavonoid compounds, such as catechin, narigenin and quercetin, significantly inhibited HCV replication [11], with quercetin inhibiting the HCV NS3 serine protease activity [12]. Further studies to identify antiviral activities of medicinal plants offer a great opportunity to find effective new drug candidates. Indonesia is said to possess the second largest biodiversity in the world, with around 40,000 endemic plant species including 6,000 medicinal plants [13]. In this study, ethanol extracts of certain Indonesian medicinal plants explored from the East Java region were evaluated for their anti-HCV activities.

Results

Anti-HCV activities of ethanol extracts of Indonesian medicinal plants

A total of 21 samples from 17 species of medicinal plants explored in the East Java region, Indonesia, were used in this study. The botanical names, the families and the parts of the plants were verified by botanists. Ethanol extracts of the plants were examined for antiviral activities against the J6/JFH1-P47 (passage 47) strain of HCV genotype 2a [14] in a cell culture system using Huh7.5 cells at a multiplicity of infection (MOI) of 0.5. The 50% inhibitory concentrations (IC_{50}), the 50% cytotoxic concentrations (CC_{50}) and selectivity indexes (SI: CC_{50}/IC_{50}) of the plant extracts are shown in Table 1. The results obtained revealed that 4 of the 21 extracts possessed potential anti-HCV activities against HCV J6/JFH1-P47 with IC_{50} being <20 μg/ml and CC_{50} being >100 μg/ml. The positive samples were: *Toona sureni* leaves (TSL; IC_{50} = 13.9 μg/ml), *Melicope latifolia* leaves (MLL; IC_{50} = 3.5 μg/ml), *Melanolepis multiglandulosa* stem (MMS; IC_{50} = 17.1 μg/ml) and *Ficus fistulosa* leaves (FFL; IC_{50} = 15.0 μg/ml). Dose-dependent anti-HCV activities of TSL, MLL, MMS and FFL extracts against the HCV J6/JFH1-P47 [14] were shown in Figure 1A.

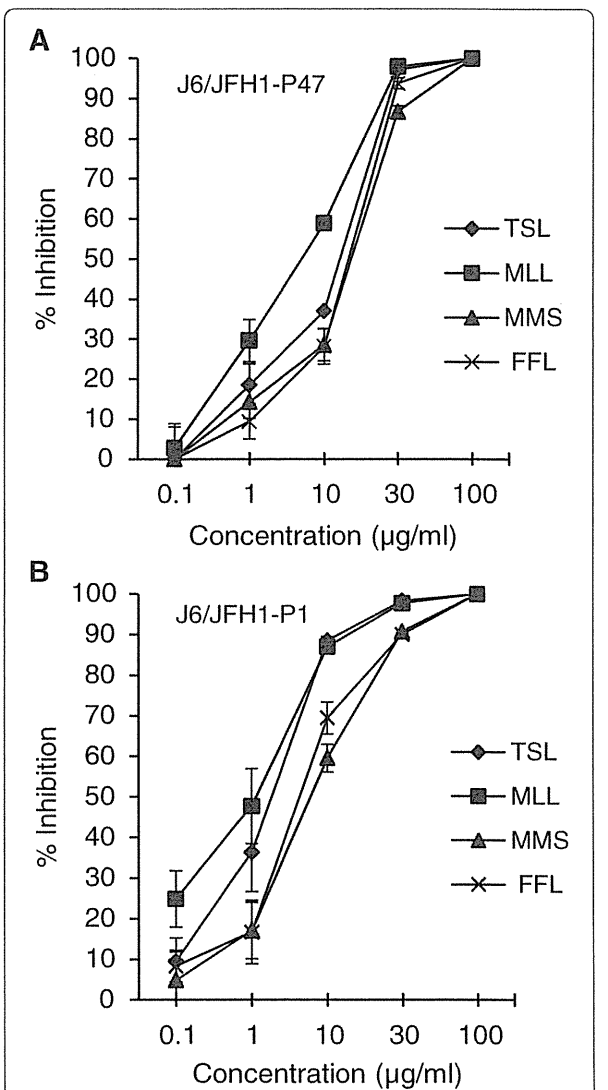

Figure 1 Dose-dependent inhibition of HCV infection by ethanol extracts of TSL, MLL, MMS and FFL. The HCV J6/JFH1-P47 **(A)** and -P1 strains **(B)** were mixed with serial dilutions of the plant extracts and inoculated to Huh 7.5 cells at an MOI of 0.5 and 0.05, respectively. After virus adsorption, the cells were cultured with the same concentrations of plant extracts for 46 hours. The culture supernatants were harvested and titrated for the virus infectivity. Percent inhibitions of HCV infectivity by the plant extracts at the concentrations of 0.1 to 100 μg/ml are shown. Data represent means ± SEM of data from two independent experiments.

Mode of action of ethanol extracts of TSL, MLL, MMS and FFL

To determine whether the anti-HCV effects of TSL, MLL, MMS and FFL extracts are exerted at the entry or the post-entry step, time-of-addition experiments were performed, in which three sets of experiments were done in parallel: (i) HCV was mixed with a plant extract (30 μg/ml) and the mixture was inoculated to the cells. After virus adsorption for 2 hours, the residual virus and the plant extract were removed, and cells were refed with fresh medium without the plant extract for 46 hours. This experiment examines the antiviral effect at the entry step. (ii) HCV was inoculated to the cells in the absence of the plant extract. After virus adsorption for 2 hours, the residual virus was removed and cells were refed with fresh medium containing the plant extract (30 μg/ml) for 46 hours. This experiment examines the antiviral effect at the post-entry step. (iii) As a positive control, HCV mixed with the plant extract was inoculated to the cells. After virus adsorption for 2 hours, the